

# Size effect on aperture and permeability of a fracture as estimated in large synthetic fractures

K. Matsuki<sup>a,\*</sup>, Y. Chida<sup>a,1</sup>, K. Sakaguchi<sup>a</sup>, P.W.J. Glover<sup>b</sup>

<sup>a</sup>Department of Environmental Studies, Graduate School of Environmental Studies, Tohoku University, 6-6-20 Aramaki-aza-Aoba, Aoba-ku, Sendai 980-8579, Japan

<sup>b</sup>Université Laval, Québec G1K 7P4, Canada

Accepted 2 December 2005

Available online 27 January 2006

## Abstract

Synthetic fractures of from 0.2 to 12.8 m in size were created on a computer by a new spectral method to reproduce the ratio of the power spectral density of the initial aperture (the aperture when the surfaces are in contact at a single point) to that of the surface height determined for a tensile fracture of 1 m. First, the size effect on the standard deviation of the initial aperture was analyzed for fractures with and without shearing. Next, by taking aperture data at constant intervals to establish a flow area, water flow was simulated for fractures during both normal closure and closure after shearing, by solving Reynolds equation to determine the hydraulic aperture. When the fracture is closed without shearing and has the same mean aperture, the effect of the fracture size on the hydraulic aperture disappears if the fracture is larger than about 0.2 m, since beyond this size the standard deviation of the initial aperture is almost independent of the fracture size. When the fracture is closed after shearing, the hydraulic conductivity shows remarkable anisotropy, which becomes more significant with both shear displacement and closure. However, the relation between the hydraulic aperture normalized by the mean aperture and the mean aperture normalized by the standard deviation of the initial aperture is almost independent of both the fracture size and shear displacement when the shear displacement is less than about 3.1% of the fracture size, at which point the standard deviation of the initial aperture of the sheared fracture is almost independent of the fracture size.

© 2006 Elsevier Ltd. All rights reserved.

**Keywords:** Size effect; Permeability; Aperture; Synthetic fracture; Closure; Shear; Power spectral density

## 1. Introduction

Evaluation of the hydraulic properties of a rock mass is a prerequisite for designing rock structures in various engineering projects such as for underground disposal of high-level radioactive wastes, underground storage of energy and geothermal energy extraction. The hydraulic properties of a rock mass are governed by those of the fractures in the rock mass, since fractures such as joints may be the main conduits for water flow [1]. Although the permeability of a fracture is mainly determined by the mean aperture of the fracture resulting from the rock stress, as often modeled in simulations of water flow, the

variation in the aperture, such as reflected by the standard deviation (SD), also plays an important role, since as the SD of the aperture increases, the effective void for water flow is reduced. Fig. 1 schematically shows the effective space for water flow for three aperture distributions with the same mean aperture ( $e_m$ ) but different SDs ( $\sigma_{01} < \sigma_{02} < \sigma_{03}$ ). While voids greater than the mean aperture do not provide an effective conduit for water flow unless they are connected to each other to form a channel, apertures smaller than the mean aperture may inhibit water flow. Thus, the mean aperture relative to the variation in the aperture may be a primary factor in determining the permeability of a normally closed fracture [2–6].

Matsuki et al. [7] measured the aperture distribution of a small-scale hydraulic fracture created in granite in the laboratory and simulated water flow by using part of the

\*Corresponding author. Tel./fax: +81 22 795 7380.

E-mail address: [matsuki@mail.kankyo.tohoku.ac.jp](mailto:matsuki@mail.kankyo.tohoku.ac.jp) (K. Matsuki).

<sup>1</sup>Present address: Honda Corporation, Japan.

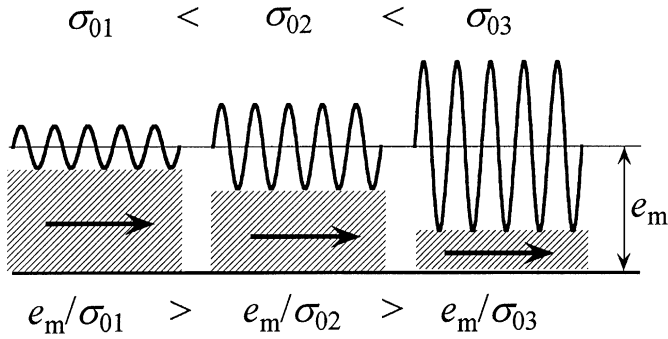


Fig. 1. Schematic of effective space for water flow for three aperture distributions with the same mean aperture ( $e_m$ ) but different standard deviations ( $\sigma_{01} < \sigma_{02} < \sigma_{03}$ ).

aperture distribution, which ranged from  $3.2 \text{ mm} \times 3.2 \text{ mm}$  to  $16 \text{ mm} \times 16 \text{ mm}$  in size. They found that the hydraulic aperture of a fracture under normal stress decreases with an increase in the flow area when the fracture is closed to have the same mean aperture, since the percentage of the contact area increases with an increase in the flow area due to the increase in the SD of the initial aperture with an increase in the flow area. A hydraulic aperture is an aperture consistent with a parallel-plates model that gives the same volume flow rate for the fracture, and the initial aperture is the aperture in which a fracture is closed to give contact at a single point. This scale effect is consistent with the experimental results obtained by Raven and Gale [8] who showed that the permeability of a natural fracture decreases with the sample size. Matsuki et al. [7] also showed that the permeability of a fracture during normal closure can be estimated by the following equation, which is independent of both the fracture size and the closure:

$$\frac{e_h}{e_m} = \sqrt[3]{1 - \frac{1.13}{1 + 0.191(2(e_m/\sigma_0))^{1.93}}} \quad (1)$$

where  $e_h$  is the hydraulic aperture,  $e_m$  is the mean aperture and  $\sigma_0$  is the SD of the initial aperture. Eq. (1) gives an average relation between the normalized hydraulic aperture ( $e_h/e_m$ ) and the normalized mean aperture ( $e_m/\sigma_0$ ), which means that the actual relation between  $e_h/e_m$  and  $e_m/\sigma_0$  for a particular aperture distribution may deviate more or less from the relation given by Eq. (1). This equation as well as other equations proposed in previous reports [2,3,6] indicates that the hydraulic aperture of a normally closed fracture is usually smaller than the mean aperture and that the hydraulic aperture normalized by the mean aperture decreases with closure of the fracture. Thus, the permeability of a fracture with rough surfaces is not simply that given by a parallel-plates model with the mean aperture of the fracture unless the mean aperture is much greater than the SD of the initial aperture and accordingly the effects of surface roughness can be neglected. However, Eq. (1) may be applicable only to a small-scale fracture under normal stress.

It is well known that remarkable shear dilation occurs when a fracture with rough surfaces is subjected to shear displacement under a small normal stress since the surfaces slide past one another. Accordingly, the permeability of a sheared fracture is much greater than that of a fracture under normal closure [9,10]. Yeo et al. [11] performed an experiment to investigate anisotropic water flow through a sheared fracture and showed that the fracture is more conductive in the direction perpendicular to the shear displacement than in that parallel to the shear displacement. Matsuki et al. [12] analyzed the initial aperture during shear deformation for a small-scale hydraulic fracture created in granite in the laboratory and showed that both the SD and the power spectral density (PSD) of the initial aperture significantly increased with shear displacement. Mitani et al. [13] showed in laboratory experiments that the anisotropy in the hydraulic conductivity of a sheared fracture is caused by the formation of ridges of contact perpendicular to the shear displacement. Recently, Fardin [14] also investigated the anisotropy in the hydraulic conductance of a sheared fracture. However, the fractures used in these studies were less than a few tens of centimeters in size. Thus, the size effect on the permeability of a sheared fracture has not yet been well clarified.

A rock mass usually contains large fractures greater than 1 m. However, as described above, most investigations in the laboratory have considered the permeability of small-scale fractures, mostly smaller than 0.5 m [8,10,11,13,15–20]. It is known that fracture surfaces can be approximated by self-affine fractals [21–25], which means that the roughness of the fracture surfaces increases with the size of the fracture according to the scaling law determined by the fractal dimension of the fracture surfaces. Therefore, the permeability of a fracture with rough surfaces may be affected by the fracture size, since the aperture distribution results from mismatching between the two surfaces and accordingly the statistical properties of the aperture, such as the SD, may depend on the fracture size. Brown [26] showed that as the fracture size increases, the variance of the composite topography (aperture) increases and quickly approaches an asymptote if the PSD of the composite topography is constant for wavelengths greater than a certain wavelength, called the mismatch length scale. By analyzing the effect of size on the SD of the initial aperture of a tensile fracture of 1 m, Sakaguchi et al. [27] suggested that the SD of the initial aperture of the tensile fracture increases with the fracture size until the fracture size exceeds 0.2 m, beyond which the size effect almost disappears. To estimate the permeability of a large fracture, we have to know the aperture distribution that results from rock stress. However, it is very difficult to measure an aperture distribution of a fracture larger than 1 m.

Fractal surfaces with a desired fractal dimension can be created on a computer by using a spectral synthesis method [28]. A fracture of any size can be created by this method

within the limits of the computer used. However, to create a realistic fracture, it is essential to consider that the two surfaces of a fracture are more or less mated at long wavelengths [29–31]. Brown [26] developed a code for creating a mated fracture in which the relative phases of the Fourier components of the two surfaces are completely independent of each other for wavelengths smaller than the mismatch length scale and are the same for wavelengths greater than the mismatch length scale. Thus, the degree of matedness of the two fracture surfaces created by this code suddenly and dramatically changes at the mismatch length scale. However, as pointed out by Glover et al. [31], the degree of matedness between the two surfaces of an actual fracture gradually increases with the wavelength [30,32,33]. Thus, Glover et al. [31] modified the Brown code so that the degree of matedness of the two surfaces may gradually increase with the wavelength. However, the parameters in their code that characterize the degree of matedness as a function of the wavelength must be determined by trial and error, and accordingly their code cannot always produce a fracture with a desired degree of matedness. Thus, it would be useful to develop a method for creating a synthetic fracture with a desired degree of matedness.

In this study, based on the distributions of the surface height and the aperture measured by Sakaguchi et al. [27] for a tensile fracture of 1 m, synthetic fractal fractures ranging from 0.2 to 12.8 m were created on a computer by a new spectral method so that the ratio of the PSD of the initial aperture to that of the surface height, determined for a tensile fracture of 1 m, may be approximately reproduced. First, the size effect on the SD of the initial aperture was analyzed for the fractures with and without shearing. The size of fractures with shearing was reduced to half of the original one due to shear offset, while that of fractures without shearing was the original one. Next, by using

aperture data at constant intervals to establish a flow area, water flow was simulated for fractures during both normal closure and closure after shearing, by solving Reynolds equation with a finite difference method to determine the hydraulic aperture.

## 2. Surface height and aperture of a tensile fracture of 1 m

Sakaguchi et al. [27] produced a tensile fracture of  $1 \text{ m} \times 0.2 \text{ m}$  parallel to the rift plane in a block of granite by indenting wedges aligned in a line along the long side (1 m) and measured the heights of the two surfaces along matched paths with a laser profilometer to determine the aperture distribution of the fracture. Since the height of the surfaces that contained transparent minerals such as quartz could not be accurately measured by the laser profilometer, they coated the surfaces of the fracture with black paint as thin and as uniformly as possible. The laser profilometer (resolution =  $30 \mu\text{m}$ ) was driven in a horizontal ( $X$ – $Y$ ) plane by a two-dimensional (2D) positioning system with two linear motor actuators (minimum step =  $1 \mu\text{m}$ ). Fig. 2 shows one of the surfaces and the initial aperture of the fracture. We took the  $X$ -axis along the short side (0.2 m) and the  $Y$ -axis along the long side (1 m). In this study, the aperture produced by surfaces that are in contact at a single point is called the initial aperture to uniquely define the aperture of a fracture when the fracture surfaces are not deformed. The measurement was performed with a step of 0.1 mm in both directions, but the figure is given with a step of 6.7 mm for convenience. Using the data, the PSDs of the linear profiles along the  $Y$ -axis were calculated by FFT (fast Fourier transform) for the two surface heights and the initial aperture, and ensemble-averaged for the two surfaces together and the initial aperture. Hereafter, we call the PSD of the linear profiles of the surface height or

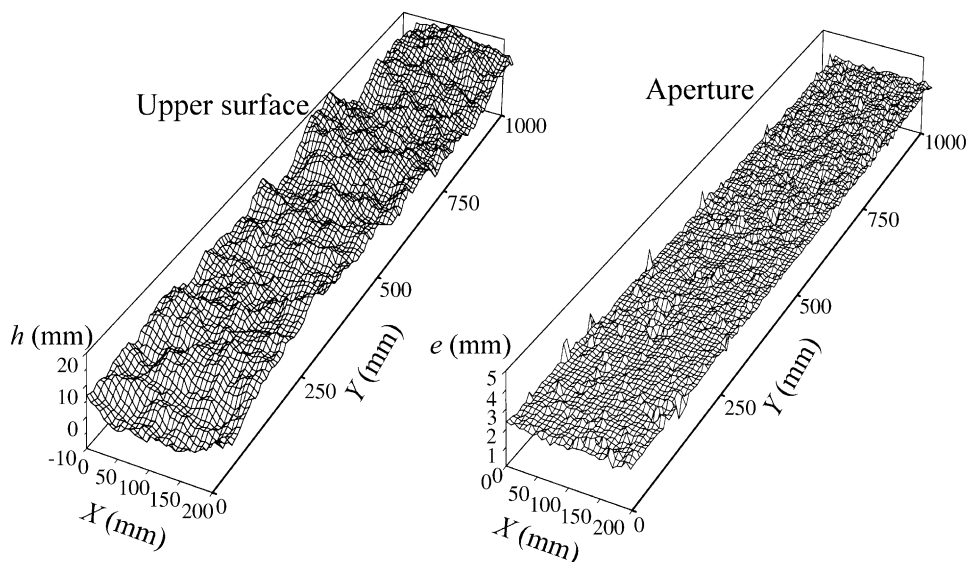


Fig. 2. Upper surface and initial aperture of a tensile fracture with a size of  $1 \text{ m} \times 0.2 \text{ m}$ .

the initial aperture simply that of the surface height or the initial aperture.

Fig. 3 shows the PSDs of the surface height and the initial aperture on a log–log plot. The wavelength is the inverse of the spatial frequency. The broken line shows the PSD of a perfectly fractal (self-affine) surface with a fractal dimension of 2.297 for reference. The fractal dimension of a surface is obtained by adding 1 to that of a linear profile if the surface is isotropic [34]. The PSD of the surface height shows linearity for spatial frequencies of from about  $4 \times 10^{-3} \text{ mm}^{-1}$  to  $0.6 \text{ mm}^{-1}$ . By comparing the PSD of the surface height of the fracture with that of a hydraulic fracture for which the surface height was measured by a profilometer with a stylus with a tip radius of  $25 \mu\text{m}$ , Sakaguchi et al. [27] concluded that the non-linearity at high frequencies mainly arose from the surface coating, which altered the components of high frequencies. On the other hand, the non-linearity at low frequencies was considered to be caused by the constraint of the direction of fracture propagation along a line when the fracture was created using aligned wedges [27]. Accordingly, the apparent cut-off of the PSD of the surface height at the lowest frequencies may disappear if the fracture propagates without this constraint. Thus, the fractal dimension of the surface height was determined by using data from within the linear portion of the surface height PSD. When the PSD of surface heights  $G(f)$  is given as a function of spatial frequency  $f$  by

$$G(f) = Af^{-\alpha}, \tag{2}$$

the fractal dimension of the surface  $D$  ( $2 < D < 3$ ) is determined by [34,35]

$$D = \frac{7 - \alpha}{2}, \tag{3}$$

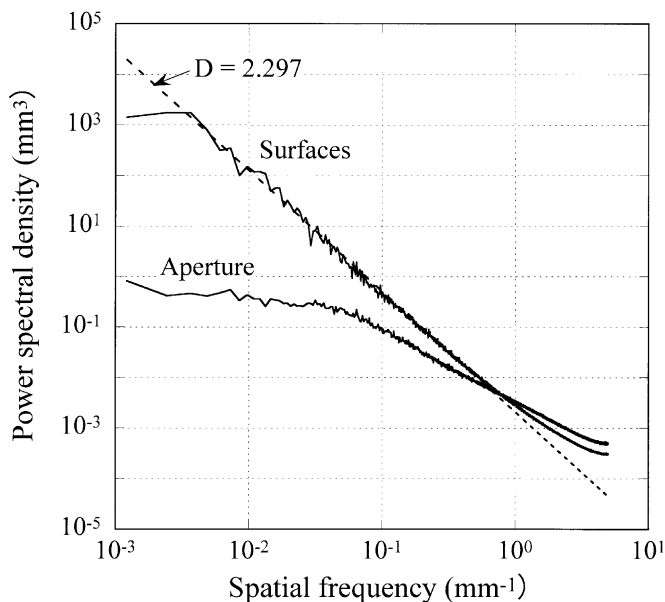


Fig. 3. Power spectral densities of the surface height and initial aperture of a tensile fracture with a size of 1 m.

where  $\alpha$  is the power in Eq. (2), determined from the slope of the log–log plot of  $G(f)$ . Thus, the fractal dimension of the fracture surfaces was determined to be 2.297, since  $\alpha$  was 2.406.

In contrast to the PSD of the surface height, that of the initial aperture does not increase with an increase in the wavelength as much as that of the fracture surfaces (Fig. 3). This means that the degree of matedness (correlation) of the two surfaces increases with an increase in the wavelength [29–31]. No apertures are produced when the two surfaces in contact are the same, while the PSD of the initial aperture is twice that of when two surfaces with the same roughness are independent of each other [23]. Thus, the ratio of the PSDs of the initial aperture and the surface height gives us a measure for evaluating the degree of matedness between two fracture surfaces [29]. Fig. 4 shows the ratio of the initial aperture PSD to the surface height PSD as a function of the spatial frequency for the tensile fracture created in granite. The ratio begins to decrease with an increase in the wavelength at a wavelength of 0.568 mm. Thus, we determined the so-called mismatch length scale ( $\lambda_c$ ) to be 0.568 mm by assuming that the surface coating does not have a significant effect on the ratio since this value is not so different from the value (0.85 mm) determined by a profilometer with a stylus with a tip radius of  $25 \mu\text{m}$  for a small-scale hydraulic fracture created in the same granite [30]. The thin line indicates a curve obtained by fitting the data for wavelengths greater than the mismatch length scale, and ignoring the data for the two greatest wavelengths. The fitted curve was extended to a wavelength of 20 m, beyond the size of the tensile fracture (1 m), to be used as a reference for creating a large synthetic fracture, as will be described later. Fig. 4 indicates that the degree of matedness of the two fracture surfaces

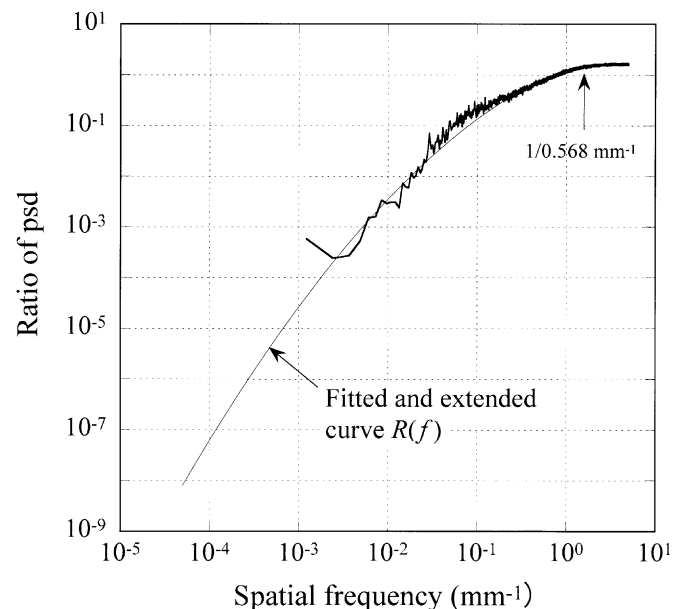


Fig. 4. Ratio of the initial aperture PSD to the surface height PSD as a function of spatial frequency for a tensile fracture in granite.

continuously increases with an increase in the wavelength when the wavelength is greater than the mismatch length scale. This explains why the two surfaces of a tensile fracture resemble each other. We will create a synthetic fractal fracture so that the ratio given by the fitted curve may be reproduced.

**3. Method for creating a synthetic fracture**

*3.1. Spectral method based on fractional Brownian motion for creating an isotropic surface*

Synthetic fractures with isotropic surfaces were created by a spectral method based on fractional Brownian motion (fBm) [28,34]. In this method, a fractal surface is created by the inverse Fourier transform of the Fourier components that are given according to the scaling law of the surface height, which is determined by the fractal dimension of the surface  $D$ . The discrete inverse Fourier transform to create an isotropic fracture surface  $h(x, y)$  of size  $L \times L$  with  $N \times N$  points is given by

$$h(x, y) = \sum_{k=0}^{N-1} \sum_{l=0}^{N-1} a_{kl} e^{i2\pi((km+ln)/N)}, \tag{4}$$

where  $a_{kl}$  is a complex Fourier component of the surface for the spatial frequencies  $k/L$  and  $l/L$  in the  $X$ - and  $Y$ -directions, respectively. Note that  $x$  and  $y$  are discretized as

$$\begin{aligned} x &= m\Delta x \quad (m = 0, N - 1), \\ y &= n\Delta y \quad (n = 0, N - 1), \end{aligned} \tag{5}$$

where  $\Delta x$  and  $\Delta y$  are the grid spacing in the  $X$ - and  $Y$ -directions, respectively ( $\Delta x = \Delta y = L/(N-1)$ ). For a real function such as surface heights, the Fourier components must satisfy the following conjugate conditions [28]:

$$\begin{aligned} a_{N-k, N-l} &= \overline{a_{kl}} \quad (k, l > 0), \\ a_{0, N-l} &= \overline{a_{0l}} \quad (l > 0), \\ a_{N-k, 0} &= \overline{a_{k0}} \quad (k > 0), \\ a_{00} &= \overline{a_{00}}, \end{aligned} \tag{6}$$

where the overbar means the conjugate of the complex. Since we assumed that the constant component  $a_{00}$  is zero, the mean height of the surface is always zero. When the fractal dimension  $D$  is determined from coefficient  $\alpha$  in Eq. (2), the Fourier component  $a_{kl}$  can be given as a function of the spatial frequency  $f \left( = \sqrt{(k^2 + l^2)}/L \right)$  in an arbitrary direction by [28]

$$a_{kl} \propto (k^2 + l^2)^{-((4-D)/2)} e^{i2\pi R_1}, \tag{7}$$

where  $R_1$  is a series of random numbers uniformly distributed from 0 to 1 to give the relative phase of the Fourier component ( $2\pi R_1$ ). The surface height was adjusted after taking the inverse Fourier transform of Eq. (7) with an arbitrary proportional constant so that

statistical properties of the surface height may be reproduced, as described below.

If  $G(f)$  is given as a continuous function of  $f$ , the variance  $\sigma_h^2$  of the surface height along a linear profile of length  $L$  is obtained by [26]

$$\sigma_h^2 = \int_{1/L}^{\infty} G(f) df, \tag{8}$$

where  $1/L$  is the minimum frequency. The variance of the surface height along a linear profile ( $\sigma_h^2$ ) is smaller than that of the whole 2D-surface height since the mean height is different for each linear profile. When  $G(f)$  is given by Eq. (2) as a continuous function of  $f$ , the variance  $\sigma_h^2$  can be obtained by taking the integral of Eq. (8):

$$\sigma_h^2 = \frac{A}{\alpha - 1} L^{\alpha-1}. \tag{9}$$

However, when  $G(f)$  is given at discrete frequencies as in this study, the discrete form of Eq. (8) can be given by

$$\sigma_h^2 = \sum_{i=1}^{\infty} \frac{1}{L} G(f_i), \tag{10}$$

where  $f_i = i/L$ . Thus, Eq. (9) does not include the full contribution at the minimum frequency, as shown in Fig. 5. An additional term of  $\frac{1}{2}G(1/L)1/L$ , which is half of the contribution at the minimum frequency ( $= 1/L$ ) and is indicated by the hatched area in Fig. 5, should be added to Eq. (9), and this is indicated by the gray area in Fig. 5. Accordingly, the variance  $\sigma_h^2$  should be given by

$$\sigma_h^2 = \frac{1}{2} \frac{\alpha + 1}{\alpha - 1} AL^{\alpha-1}. \tag{11}$$

From Eqs. (3) and (11), the scaling law for the SD of the height of a fractal surface determined along a linear profile  $\sigma_h$  can be given by

$$\sigma_h = \sigma_{h0} \left( \frac{L}{L_0} \right)^{3-D}, \tag{12}$$

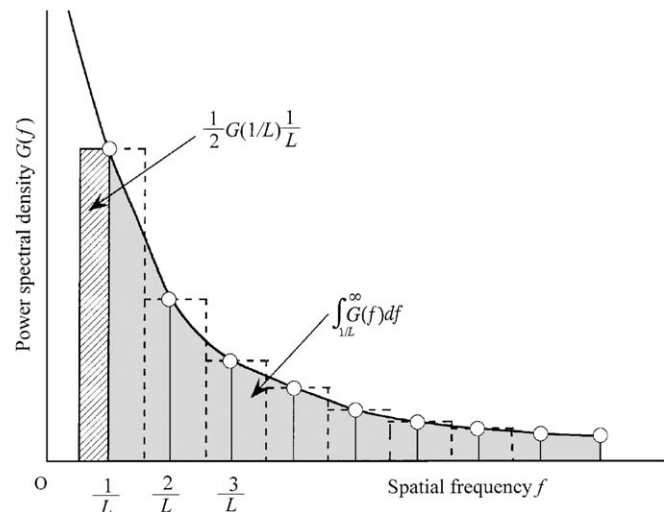


Fig. 5. Estimation of the variance in a linear profile of surface height for a discrete power spectral density.

where  $\sigma_{h0}$  is the SD of the surface height along a linear profile of a fracture surface of size  $L_0$ .

In this study, the surface height was adjusted after taking the inverse Fourier transform of Eq. (7) so that the average SD determined for all linear profiles of the surface height ( $\sigma_h$ ) may coincide with the value given by Eq. (12), since the PSD of the linear profile of the surface height must be reproduced to reproduce the measured ratio of the initial aperture PSD to the surface height PSD (Fig. 4). In Eq. (12), we used a reference fracture size of 0.2 m and the measured value of  $\sigma_{h0}$ . If the surface height is adjusted so that the variance of the 2D surface height is the same as that of the measured value, the coefficient  $A$  in Eq. (2) of the synthetic fracture does not always coincide with the measured value. Thus, one of the fracture surfaces, say the upper surface, can be created with a designated roughness for the linear profiles of the surface height ( $\sigma_h$ ) and the fractal dimension ( $D$ ).

### 3.2. Method for creating the other surface

The other (lower) surface of a fracture must be created by considering a gradual increase in the matedness between the two surfaces for wavelengths greater than the mismatch length scale ( $\lambda_c$ ), as described previously. This can be accomplished by introducing Fourier components for the lower surface with the same amplitude as that of the upper surface but with a different relative phase from that of the upper surface. Thus,  $a_{kl}$  of the lower surface is given by

$$a_{kl} \propto (k^2 + l^2)^{-(4-D)/2} e^{i(2\pi R_1 + 2\pi\gamma(f)R_2)}, \quad (13)$$

where  $R_2$  is a series of random numbers that is independent of  $R_1$  in Eq. (7) for the upper surface, and  $\gamma(f)$  is a function of the spatial frequency  $f$ , which is equal to or less than 1. Thus, the difference in phases between the two fracture surfaces is given by  $2\pi\gamma(f)R_2$  for which

$$\gamma(f) = \begin{cases} 1 & (f \geq f_c), \\ \gamma(f) & (f < f_c), \end{cases} \quad (14)$$

where  $f_c$  is the inverse of the mismatch length scale ( $= 1/\lambda_c$ ). We assumed that the heights of the two surfaces are given from the same reference plane for convenience. Accordingly one of the two surfaces is a mirror image of the real one.

Let us consider the effect of the phase difference on the ratio of the initial aperture PSD to the surface height PSD. The Fourier component of the initial aperture is obtained by taking the difference between those of the upper and lower surfaces since the surface heights are given by the distance from the same reference plane. Thus, the Fourier component of the aperture  $e_{kl}$  is given by

$$e_{kl} \propto (k^2 + l^2)^{-(4-D)/2} e^{i2\pi R_1} (1 - e^{i2\pi\gamma(f)R_2}). \quad (15)$$

Since the PSD is a squared amplitude of the Fourier component, the ratio of the PSDs between the initial

aperture and the surface height  $r(f)$  is given by

$$r(f) = 2\{1 - \cos(2\pi\gamma(f)R_2)\}. \quad (16)$$

The ratio is zero when there are no differences in the phases ( $\gamma(f) = 0$ ), which means that there are no apertures between identical surfaces in contact. Since the expectation of the ratio  $E(r)$  is obtained by the following integral with respect to the random number  $R_2$ ,

$$E(r) = \int_0^1 r(f) dR_2, \quad (17)$$

$E(r)$  is obtained as

$$E(r) = \begin{cases} 2 & (f \geq f_c), \\ 2\left(1 - \frac{\sin 2\pi\gamma(f)}{2\pi\gamma(f)}\right) & (f < f_c). \end{cases} \quad (18)$$

Thus, the expectation of the ratio is two for spatial frequencies greater than  $f_c$  where the two surfaces are completely independent of each other, and less than two for spatial frequencies less than  $f_c$  where the two surfaces are more or less correlated with each other. Accordingly, if the function  $\gamma(f)$  is given by solving the following equation according to the measured (and extended) value  $R(f)$  (Fig. 4) for spatial frequencies less than  $f_c$ ,

$$2\left(1 - \frac{\sin 2\pi\gamma(f)}{2\pi\gamma(f)}\right) = R(f), \quad (19)$$

the ratio of the PSDs of the linear profiles between the initial aperture and the surface height may statistically satisfy the given ratio  $R(f)$ . The function  $\gamma(f)$  can be determined by an iterative method such as the Newton–Raphson method.

Synthetic fractures created by the method described above for a certain size have the same values for the roughness and fractal dimension of the surfaces, the degree of matedness between the surfaces, the average PSDs of the surface height and the initial aperture, and the SD of the initial aperture. Thus, the synthetic fracture is statistically unique, while the layout of the aperture of each fracture can be changed by using different series of the random numbers for  $R_1$  and  $R_2$ . In this study, we did not use the same series of the random numbers for all fractures to investigate the effect of the aperture layout on the permeability.

### 3.3. Effect of grid spacing on the variance of the surface height and the aperture

In creating a synthetic fracture, we will use a certain value of grid spacing. Therefore, a significant error in the variance of the surface height or that of the initial aperture may be produced if we use large grid spacing, even if the PSDs of the initial aperture and the surface height are reproduced. When the number of grid points is  $N \times N$  for a square fracture of size  $L \times L$ , the maximum frequency contained in the synthetic fracture is  $(N-1)/L$ , since the

grid spacing is  $L/(N-1)$ . An error in the variance of the surface height due to the cut-off of frequencies greater than  $(N-1)/L$  is obtained by integrating  $G(f)$  (Eq. (2)) from  $(N-1)/L$  to infinity and is given by

$$\Delta\sigma_h^2 = \frac{A}{\alpha - 1} \left( \frac{N-1}{L} \right)^{1-\alpha} \quad (20)$$

Accordingly, an error relative to the variance of the surface height  $\sigma_h^2$  is obtained from Eqs. (11) and (20).

$$\frac{\Delta\sigma_h^2}{\sigma_h^2} = \frac{2}{\alpha + 1} \frac{1}{(N-1)^{\alpha-1}} \quad (21)$$

The above equation indicates that the relative error in the variance of the surface height is independent of the fracture size and that  $N$  of 128 is sufficient to give a relative error of less than 0.1% when  $\alpha$  is 2.406. This is because the amplitude of the fractal surfaces rapidly decreases with an increase in the spatial frequency (Fig. 3).

The effect of grid spacing on the variance of the initial aperture can be estimated in a similar manner as described above. However, the rate of the increase in the PSD of the initial aperture with respect to the increase in the wavelength decreases with the wavelength (Fig. 3), which suggests that the cut-off of high frequencies may have a more significant effect on the variance of the initial aperture. Since the PSD of the initial aperture is given by  $G(f)R(f)$ , the variance of the initial aperture  $\sigma_{e0}^2$  along a linear profile for a fracture of size  $L$  is obtained by integrating  $G(f)R(f)$  from  $1/L$  to infinity, while the variance of the initial aperture  $\sigma_e^2$  with the cut-off frequency  $(N-1)/L$  is given by integrating  $G(f)R(f)$  from  $1/L$  to  $(N-1)/L$ . Thus, the ratio between them in the discrete form of the integral is

$$\sigma_e^2/\sigma_{e0}^2 = \frac{1}{L} \sum_{i=1}^{N-1} G(f_i)R(f_i) \left/ \left\{ \frac{1}{L} \sum_{i=1}^{\infty} G(f_i)R(f_i) \right\} \right. \quad (22)$$

where  $f_i = i/L$ . Fig. 6 shows the ratio  $\sigma_e^2/\sigma_{e0}^2$  as a function of cut-off frequency for the maximum (12.8 m) and minimum (0.2 m) fracture sizes adopted in this study. When the cut-off frequency is greater than  $5 \text{ mm}^{-1}$ , the variance of the initial aperture is more than 99.5% of the theoretical value for a fracture size of 12.8 m and more than 99.2% for a fracture size of 0.2 m. Thus, for all fracture sizes used in this study, the grid spacing was determined to be less than 0.2 mm to reproduce the variance of the initial aperture along a linear profile with an error of less than 0.8%, which corresponds to an error in the SD of the initial aperture of less than 0.4%. Thus, large synthetic fractures were created with a huge number of grid points. However, as will be described later, we took aperture data at intervals to establish a flow area for simulating water flow, due to the limited capability of existing computers.

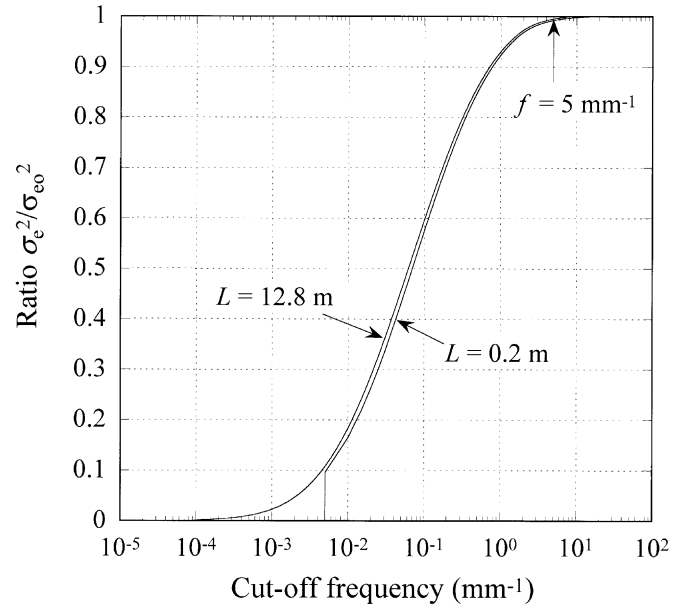


Fig. 6. Effect of cut-off frequency on the ratio of variance in a linear profile of the initial aperture.

#### 4. Created synthetic fractures

##### 4.1. Surfaces and aperture of a fracture without shear deformation

Seven square fractures with sizes of 0.2, 0.4, 0.8, 1.6, 3.2, 6.4 and 12.8 m were created with a grid spacing of about 0.2 mm by the method described above. Table 1 shows the parameters used in this study for creating the fractures. These parameters were determined based on measured data for a square area of  $0.2 \text{ m} \times 0.2 \text{ m}$  of a tensile fracture in granite [27]. The grid points for both the  $X$ - and  $Y$ -directions were  $2^{10}$  ( $= 1024$ ),  $2^{11}$ ,  $2^{12}$ ,  $2^{13}$ ,  $2^{14}$ ,  $2^{15}$  and  $2^{16}$  ( $= 65536$ ) for fracture sizes of 0.2, 0.4, 0.8, 1.6, 3.2, 6.4 and 12.8 m, respectively. Thus, the grid spacing ranged from 0.1953 to 0.1955 mm, and in all cases was less than 0.2 mm. The SD of the linear profiles of the two fracture surfaces was determined according to the scaling law given by Eq. (12) ( $D = 2.297$ ,  $\sigma_{h0} = 1.966 \text{ mm}$  and  $L_0 = 0.2 \text{ m}$ ). Thus, the roughness of the fracture surfaces significantly increases with size. Fig. 7 shows the upper surfaces of these synthetic fractures. The lower surface of each fracture looks almost identical to the upper surface and accordingly we do not show them. The number of grid points was greatly reduced for convenience and the scale of the surface height increases with the fracture size. Note that since we cannot show the figures with a size proportional to the fracture size, the surface height distribution only gives the appearance relative to each fracture size. Since these surfaces are self-affine fractals with the same fractal dimension, the surface height relative to the fracture size looks similar for all fractures when an appropriate scale of the surface height is adopted for each fracture size. The

Table 1  
Parameters used to create synthetic fractures

Fracture size (m)	0.2	0.4	0.8	1.6	3.2	6.4	12.8
Standard deviation of linear profile of surface height (mm)	1.966	3.148	5.114	8.307	13.495	21.923	35.663
Number of grid points in X- and Y-axes	1024	2048	4096	8192	16384	32768	65536
Grid spacing $\Delta x = \Delta y$ (mm)	0.1953–0.1955						
Fractal dimension	2.297						
Mismatch length scale (mm)	0.568						

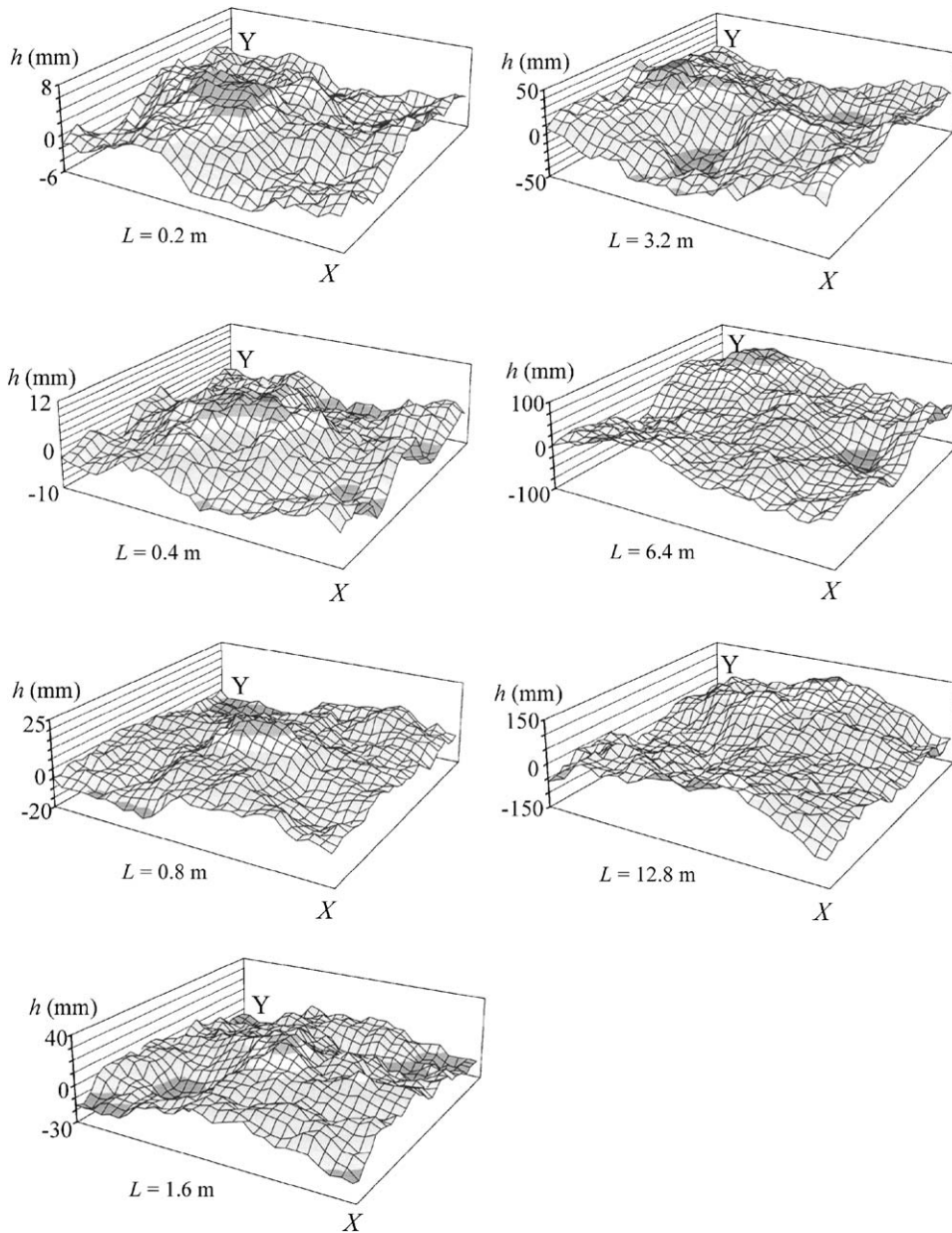


Fig. 7. Upper surfaces of synthetic fractures of from 0.2 to 12.8 m in size.

initial aperture distribution is shown in Fig. 8. The scales of the aperture in these figures are the same for all fracture sizes since the mean initial aperture only slightly increases with the fracture size. The initial aperture distributions relative to the fracture size look similar for all fracture sizes

even when the same scale of the aperture is used for all fractures. Thus, the initial aperture produced by the two self-affine fractal surfaces is no longer fractal.

Fig. 9 shows the average PSD of the heights of the two surfaces and that of the initial aperture for all synthetic

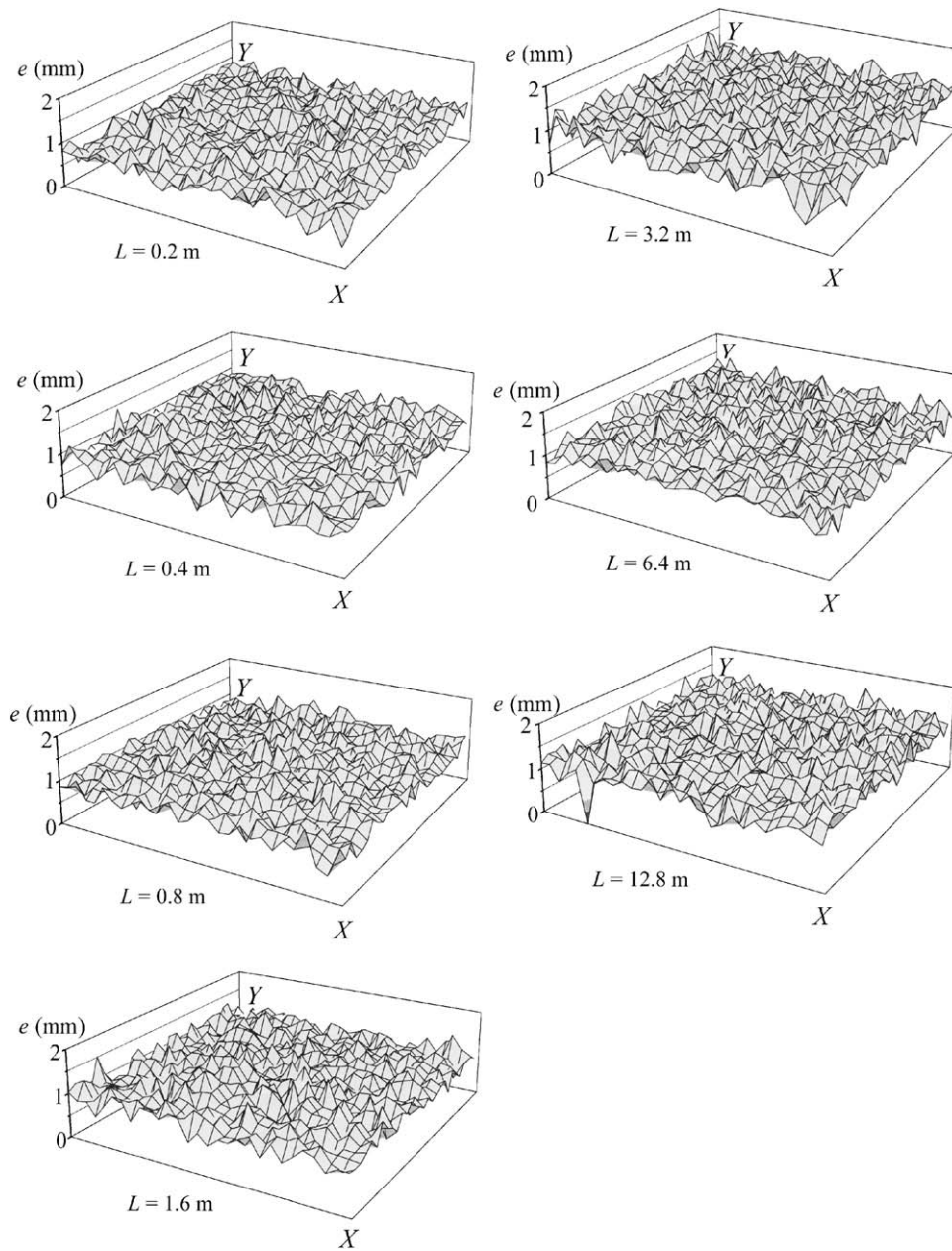


Fig. 8. Initial aperture distribution of the synthetic fractures from 0.2 to 12.8 m in size.

fractures in comparison with those for the tensile fracture in granite (thin lines) (Fig. 3). The range of the spatial frequency is shown for each fracture size. The measured PSDs of the surface height and the initial aperture of the tensile fracture were approximately reproduced by the synthetic fractures. The ratio of the PSDs of the initial aperture and the surface height is shown in Fig. 10, with a curve of  $R(f)$  for reference. The ratio for the synthetic fractures is only slightly greater than  $R(f)$  on the log–log plot. Thus, the method for creating a synthetic fracture proposed in this study has been proved to be useful for creating a realistic fracture with a desired degree of mateness.

The SD of the 2D surface height and the SD of the (2D) initial aperture of the synthetic fractures are summarized in

Table 2 and are also shown in Fig. 11 as a function of the fracture size on a log–log plot. These values for fracture sizes of less than 0.2 m (0.1, 0.05, 0.025 and 0.0125 m), the mean SD of the linear profiles of the surface height and the mean values and ranges of the SDs of both the 2D surface height and the (2D) initial aperture measured for an area of  $0.2\text{ m} \times 0.2\text{ m}$  of the reference tensile fracture are also shown for comparison. The SDs of both the 2D surface height and the initial aperture approximately reproduced the measured values. The logarithm of the SD of the 2D surface height is linear with the logarithm of the fracture size and has the same slope as that of the SD of the linear profiles, although the SD of the 2D surface height is about 1.21 times that of the linear profiles. Thus, Eq. (12) also gives the scaling law for the SD of the 2D surface height,

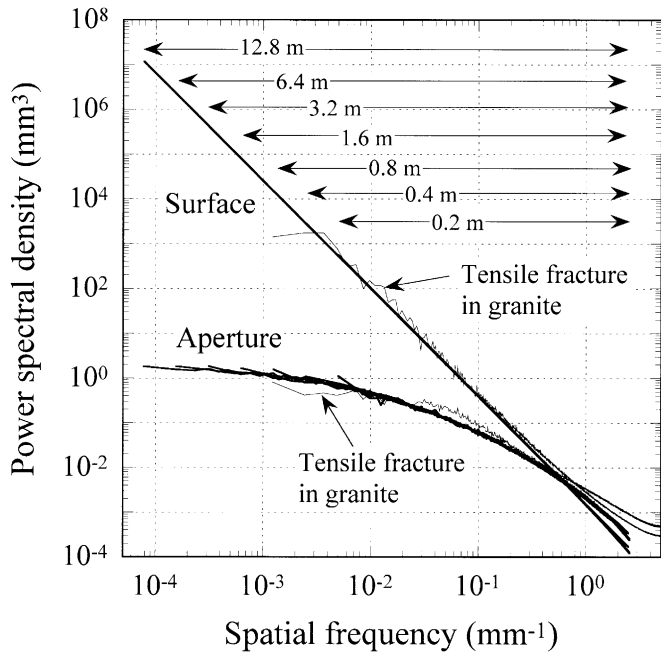


Fig. 9. Average PSDs of the surface height and the initial aperture for all synthetic fractures in comparison with measured values.

since it is normalized by the value of a reference fracture size.

In contrast to the SD of the surface height, the SD of the initial aperture is almost constant for fracture sizes greater than 0.2 m. By analyzing the size effect on the SD of the initial aperture of a tensile fracture created in granite, Sakaguchi et al. [27] suggested that the SD of the initial aperture of the tensile fracture increases with fracture size until the fracture size exceeds 0.2 m, beyond which the size effect disappears, as described previously. Thus, our synthetic fractures reproduced the same trend in the fracture size effect. Since the PSD of the initial aperture does not increase significantly at large wavelengths (Fig. 3), the contribution to the increase in the variance of (the linear profile of) the initial aperture in the integral of the PSD becomes small at large wavelengths, since the spatial frequency is very small at large wavelengths. Accordingly, the size-independence of the SD of the initial aperture may extend to a fracture size greater than 12.8 m, since the PSD of the initial aperture is not likely to significantly increase beyond the fracture size, although the size effect on the SD of the initial aperture may cease to exist if the fracture surfaces cease to be fractal at a greater size. This size effect

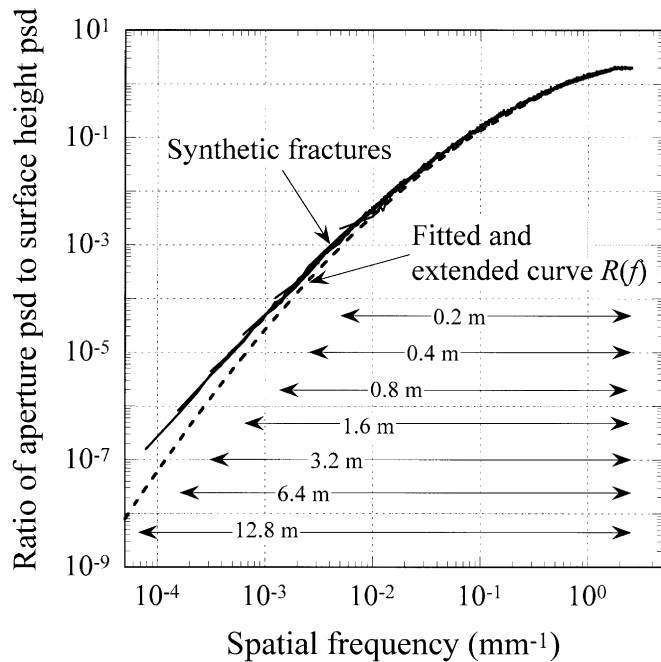


Fig. 10. Ratio of the initial aperture PSD to the surface height PSD for all synthetic fractures.

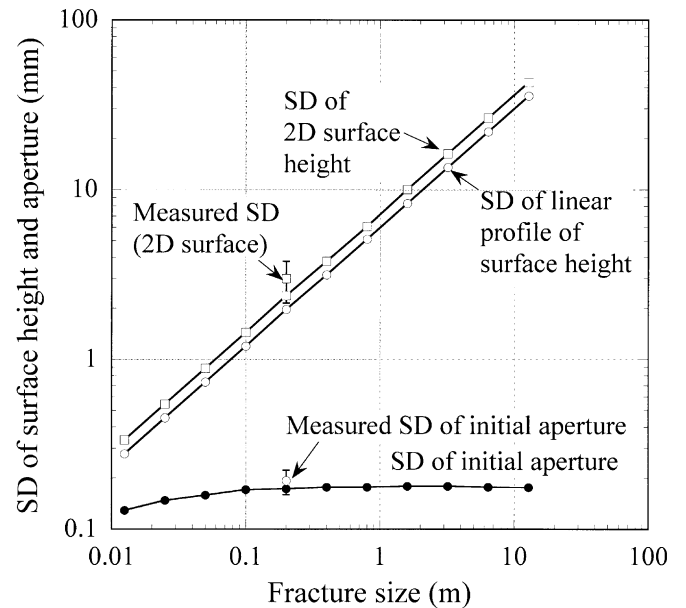


Fig. 11. Standard deviations (SDs) of 1D and 2D surface heights and SD of the initial aperture of synthetic fractures in comparison with measured values of the mean and ranges of SDs of both 2D surface height and the initial aperture.

Table 2  
Standard deviations of both the 2D surface height and 2D initial aperture of synthetic fractures

Fracture size (m)	0.2	0.4	0.8	1.6	3.2	6.4	12.8
Standard deviation of 2D surface height (mm)	2.371	3.791	6.073	10.020	16.278	26.445	42.958
Standard deviation of 2D initial aperture (mm)	0.173	0.177	0.177	0.179	0.179	0.177	0.176

on the SD of the initial aperture is important in estimating the size effect on the permeability of a large fracture when the fracture is not subjected to shear displacement because the SD of the initial aperture as well as the mean aperture may play important roles on the hydraulic conductivity of the fracture, as described previously.

#### 4.2. Aperture of a fracture subject to shear deformation

Shear displacements of 12.5, 25 and 50 mm were applied in the  $X$ -direction to the upper surface of a fracture which was then allowed to contact the lower surface by applying closure from an initial state in which the two surfaces were in contact at a single point. Thus, we avoided breaking asperities during shear deformation. This means that the fracture was sheared under a very small normal stress and the normal stress was then increased. In reality, the surfaces of a fracture would be more or less damaged when the fracture is sheared under normal stress, depending on several factors such as the normal and shear stresses, elastic constants and the tensile and compressive strengths in addition to the geometry of the fracture surfaces. Accordingly, the aperture distribution would be affected by the damage of the surfaces. However, we ignored this effect for simplicity since there are no established methods for estimating this effect and since the damage may not significantly affect the volume of the void space if the debris produced by the damage remains there.

The aperture was determined for the area common to the two surfaces. However, since shear-offset reduced the aperture data according to shear displacement, aperture data for sheared fractures were taken from only a square area with a side length of half of the original fracture size (a quarter of the original fracture area) to keep the ratios among the sheared fractures the same as those among the original fractures. Thus, the sizes of sheared fractures were reduced to half of the original values (0.1, 0.2, 0.4, 0.8, 1.6, 3.2 and 6.4 m). Hereafter, we will use these values as the size ( $L$ ) of the sheared fractures. Fig. 12 shows examples of the initial aperture distribution when the fractures are sheared by 12.5 and 50 mm. Note that the scale of the aperture for a shear displacement of  $\delta = 50$  mm is twice that with  $\delta = 12.5$  mm and that the grid lines were greatly reduced. As the shear displacement increases or as the fracture size decreases, the magnitudes of components with low frequencies (large wavelengths) in the aperture increase relative to those with high frequencies. Accordingly, the aperture distribution relative to the fracture size more closely resembles the surface of a fracture (Fig. 7) as the fracture size decreases or as the shear displacement increases. However, for large fractures, the aperture distributions relative to the fracture size remain similar to those of fractures without shear deformation (Fig. 8), although the mean aperture is much greater. Thus, the waviness (undulation with large wavelengths) of the initial aperture distribution relative to the size of the sheared

fracture is governed by the magnitude of the shear displacement relative to the fracture size.

Fig. 13 shows the effects of both the fracture size ( $L$ ) and the shear displacement ( $\delta$ ) on the SD of the initial aperture. The SD of the initial aperture for fractures without shear deformation is also shown for comparison. The broken line indicates the relation between the fracture size and the SD of the initial aperture when the shear displacement is about 3.1% of the fracture size (except for  $\delta = 0$  mm). The SD of the initial aperture significantly increases with shear displacement. On the other hand, for each shear displacement, although the SD of the initial aperture is more or less scattered, it gradually increases with fracture size until the fracture size exceeds the broken line, beyond which the SD of the initial aperture is approximately constant. The rate of the increase with respect to fracture size increases with shear displacement. Fig. 14 shows the effects of both fracture size and shear displacement on the mean initial aperture (shear dilation). The broken line indicates the same as that in Fig. 13. Similar to the SD of the initial aperture, the mean initial aperture significantly increases with shear displacement, and increases with fracture size until it exceeds the broken line, beyond which there is only a slight increase in the mean aperture, although the mean initial aperture is more or less scattered. The rate of the increase with respect to fracture size remarkably increases with shear displacement. Thus, the fracture size effect on both the shear dilation and the SD of the initial aperture almost disappears when the shear displacement is less than about 3.1% of the fracture size ( $\delta/L < 0.031$ ).

Since shear displacement decreases the degree of matedness between the two fracture surfaces, the SD of the initial aperture increases with shear displacement. Thus, shearing is a process in which there is a decrease in the degree of matedness between the two surfaces of a fracture [12]. Accordingly, the amplitudes of components of an aperture with large wavelengths, which were small for the original aperture without shearing because of the well-mated surfaces, increase with shear displacement. The effect of shear displacement on the PSD of the initial aperture of a sheared fracture will be discussed later.

## 5. Method for estimating the permeability of a fracture

### 5.1. Reynolds equation and hydraulic aperture

Three-dimensional (3D) flow of an incompressible and viscous fluid such as water is governed by the Navier–Stokes equations. However, it is beyond the capability of existing supercomputers to solve the equations for water flow through an aperture between two rough surfaces since huge amounts of memory are necessary to appropriately consider the effect of the surface roughness. Therefore, the problem has often been approximated using a 2D field by introducing the mean velocities across the aperture, and

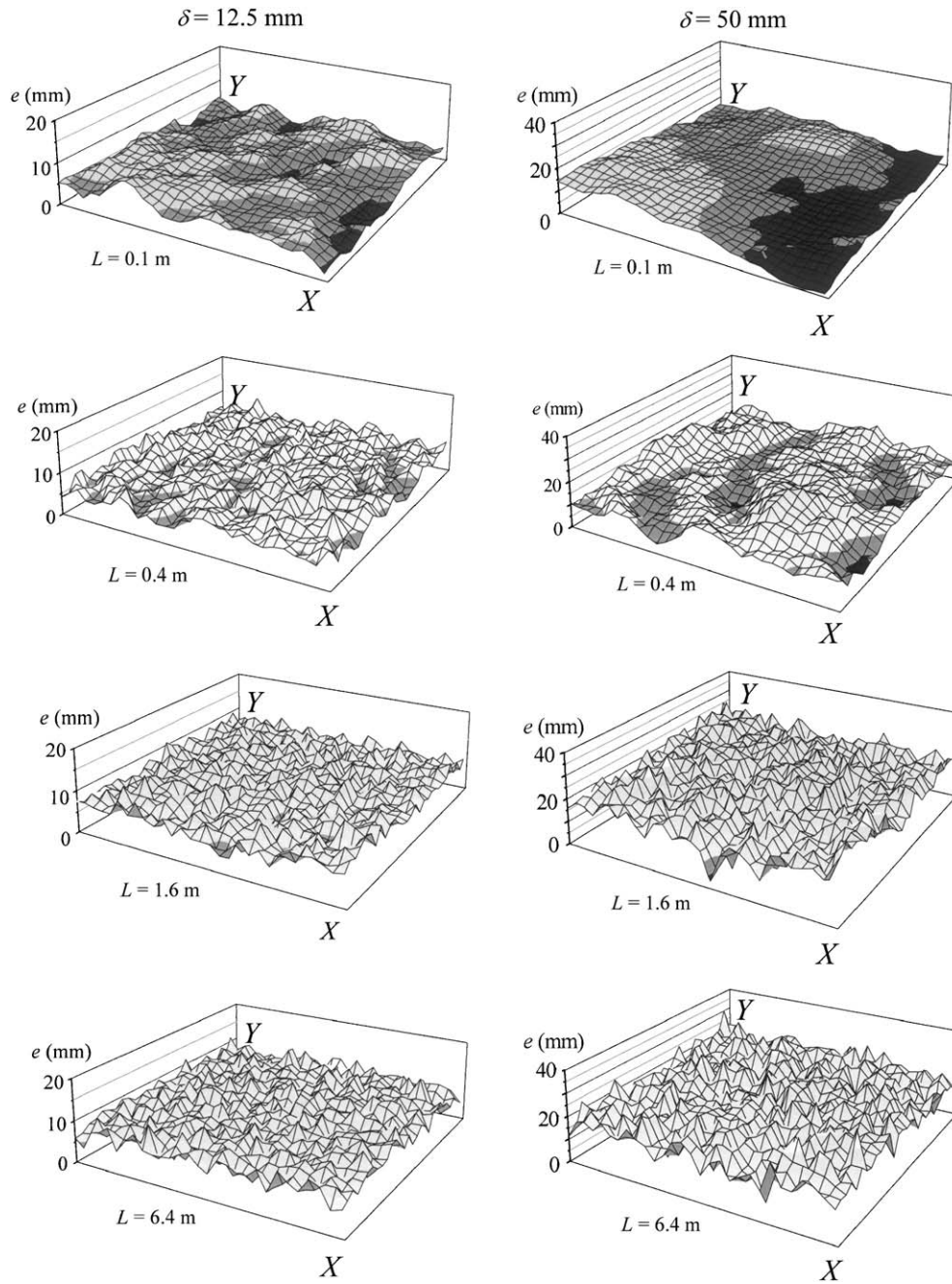


Fig. 12. Examples of the initial aperture distribution when fractures are sheared by 12.5 and 50 mm for fracture sizes of 0.1, 0.4, 1.6 and 6.4 m.

ignoring the tortuosity of the flow across the aperture. By integrating the equation of continuity across the aperture (Z-direction), we obtain the following equation in the X–Y domain:

$$\frac{\partial(eu)}{\partial x} + \frac{\partial(ev)}{\partial y} = 0, \tag{23}$$

where  $e$  is an aperture and  $u$  and  $v$  are the mean velocities in the X- and Y-directions, respectively. Furthermore, we assume that the flow at a local point can be approximated by that through parallel plates with an aperture  $e$  at that

point. Thus, the following equations were assumed to hold locally:

$$\begin{aligned} u &= -\frac{e^2}{12\mu} \frac{\partial p}{\partial x}, \\ v &= -\frac{e^2}{12\mu} \frac{\partial p}{\partial y}, \end{aligned} \tag{24}$$

where  $\mu$  is the viscosity of the fluid and  $p$  is the pressure. By substituting Eq. (24) into Eq. (23), the following equation, called Reynolds equation, is obtained for laminar flow

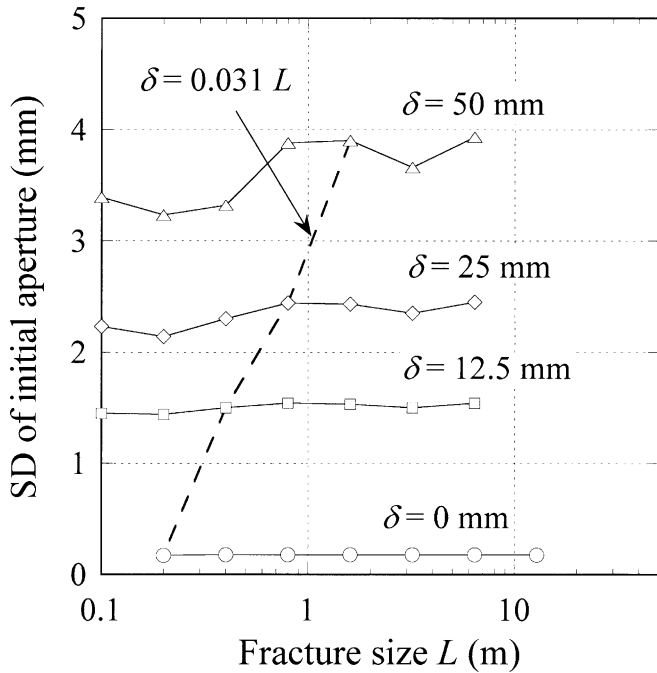


Fig. 13. Effects of both fracture size ( $L$ ) and shear displacement ( $\delta$ ) on the SD of the initial aperture.

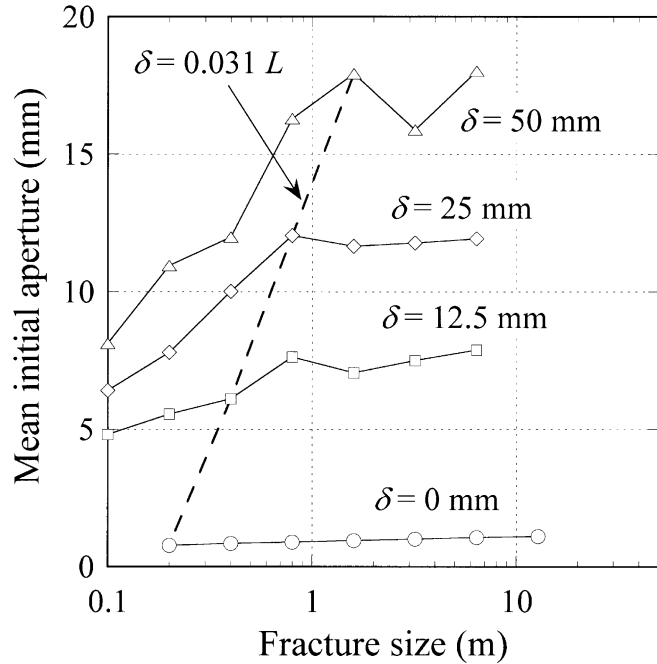


Fig. 14. Effects of both fracture size and shear displacement on the mean initial aperture (shear dilation).

through a fracture with rough surfaces [3,4,7,12,31–33]:

$$\frac{\partial}{\partial x} \left( \frac{e^3}{12\mu} \frac{\partial p}{\partial x} \right) + \frac{\partial}{\partial y} \left( \frac{e^3}{12\mu} \frac{\partial p}{\partial y} \right) = 0. \tag{25}$$

Since we assumed that  $\mu$  is constant throughout the field, this parameter can be removed from Eq. (25). Thus, by solving Reynolds equation under given boundary conditions with a finite difference method, the 2D velocity field was determined by substituting the solution of the pressure into finite difference expressions of Eq. (24). Although the Reynolds equation would tend to overestimate the velocity when the contact area is well developed [36], we used the equation since it is a practical tool for estimating the conductivity of a large fracture.

Linear equations derived from the finite difference form of the Reynolds equation were constructed by removing points in contact where the aperture is zero and accordingly the pressure cannot be defined, and the pressure distribution was solved by the Gauss–Seidel method [7]. The boundary conditions were given so that macroscopic water flow may occur in one direction, as shown in Fig. 15, where macroscopic flow is given in the  $X$ -direction as an example. To compare the velocity fields for all fracture sizes, a pressure difference at the boundaries perpendicular to the direction of the macroscopic flow is given so that the macroscopic pressure gradient might be the same for all fracture sizes. Thus, the pressure difference is given proportional to the fracture size. For boundaries parallel to the direction of the macroscopic flow, the condition of no flow across the boundaries is given, as shown in Fig. 15.

If the velocity field is determined, the volume flow rate  $Q$  is obtained by the following equation for macroscopic flow in the  $X$ -direction:

$$Q = \int_0^{L_y} eu \, dy, \tag{26}$$

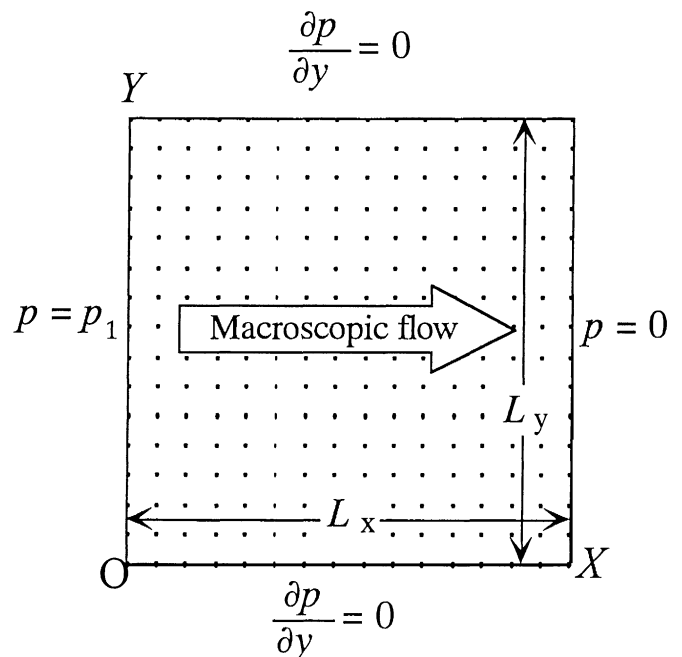


Fig. 15. Boundary conditions in the simulation of water flow.

where  $L_y$  is the length of the boundary perpendicular to the macroscopic flow ( $= L$ ) (Fig. 15). The hydraulic aperture is often used as a measure for evaluating the permeability of a fracture. It is the aperture of a parallel-plates model that gives the same volume flow rate as that of a fracture with rough surfaces. Thus, the hydraulic aperture  $e_h$  is given by [3]

$$e_h = \sqrt[3]{\frac{12\mu Q}{L_y(\Delta p/L_x)}} \quad (27)$$

where  $L_x$  is the length of the boundary parallel to the macroscopic flow ( $= L$ ) and  $\Delta p/L_x$  is the macroscopic pressure gradient. When the hydraulic aperture  $e_h$  is equal to the mean aperture of the fracture  $e_m$ , the permeability of the fracture is equivalent to that of a parallel-plates model with the same mean aperture as the fracture. Thus, the hydraulic aperture normalized by the mean aperture  $e_h/e_m$  is a useful measure for evaluating the permeability of a fracture in comparison with the permeability of a parallel-plates model with the same mean aperture. Therefore, we used the normalized hydraulic aperture  $e_h/e_m$  as a measure of the hydraulic conductivity of the fracture. Once the mean aperture  $e_m$  is determined by considering rock stress and the mechanical properties of rock, the hydraulic aperture  $e_h$  is obtained by multiplying the normalized hydraulic aperture  $e_h/e_m$  by the mean aperture  $e_m$ . Note that the normalized hydraulic aperture does not give the hydraulic conductivity itself.

5.2. Simulation of water flow

Water flow was simulated for both normal closure and closure after shearing, as described previously. During closure of the fracture, the aperture of the overlapped area was simply set to zero. In reality, the surfaces would deform at the asperities in contact, decreasing the aperture near the contacts more than is assumed in this study. Accordingly, the hydraulic conductivity of the fracture would be overestimated. However, Brown [4] showed that this effect is relatively small when the aperture is calculated, following Pyrak-Nolte et al. [37], by distributing the volume of overlapping material uniformly over the open part of the fracture. Furthermore, in reality, closure of a fracture would occur with mechanical interactions among the asperities in contact, which may cause the surfaces to tilt relative to each other and accordingly bias the aperture distribution. However, since tilting of the surfaces occurs depending on each layout of the aperture in addition to

mechanical properties of rock and the stiffness of the rock body around the fracture, it may be difficult to conclude something general. Therefore, we ignored this effect for simplicity, assuming that the reference planes for the two surfaces of a fracture are closed uniformly.

The macroscopic water flow was given in the  $X$ -direction for normal closure. For closure after shearing, the shear displacement was given in the  $X$ -direction, and water flow was analyzed for macroscopic flow in two directions: parallel ( $X$ ) and perpendicular ( $Y$ ) to the shear direction. The simulation was carried out with only  $256 \times 256$  grid points for all fractures both with and without shearing since existing supercomputers are not capable of solving Eq. (25) if all of the original data of the aperture are used. The aperture data were taken from the original data at constant intervals according to the fracture size so that the statistical properties of the aperture might not change appreciably. Accordingly, the grid spacing increased with the fracture size. The grid spacing and fracture size are summarized in Table 3. The grid spacing ranged from 0.784 to 50.196 mm for normal closure for fracture sizes of from 0.2 to 12.8 m and from 0.392 to 25.098 mm for sheared fractures for fracture sizes of from 0.1 to 6.4 m.

Fig. 16 shows a comparison of the probability density function (PDF) of the initial aperture of fractures without shearing using the original data and the data of  $256 \times 256$  points. Thick lines indicate the PDF of the original data and thin lines indicate that of the  $256 \times 256$  data. The PDF

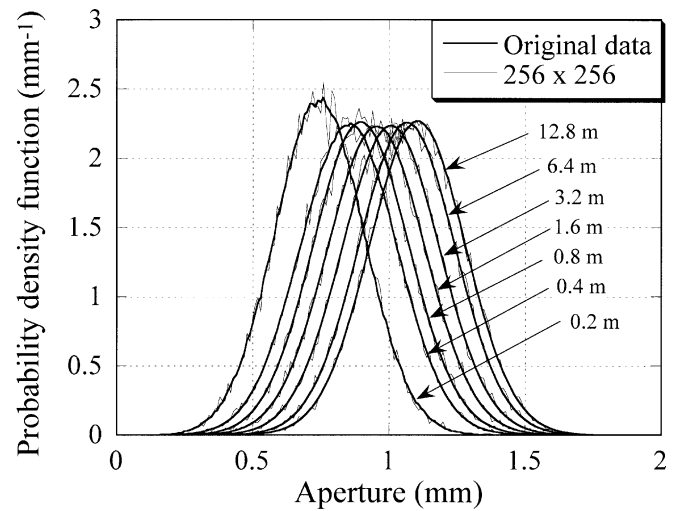


Fig. 16. Comparison of the probability density function of the initial aperture for fractures without shearing for the original data and the data using  $256 \times 256$  points.

Table 3  
Fracture size and grid spacing in the simulation of water flow

Normal closure	Fracture size (m)	0.2	0.4	0.8	1.6	3.2	6.4	12.8
	Grid spacing (mm)	0.784	1.569	3.137	6.275	12.549	25.098	50.196
Closure after shearing	Fracture size (m)	0.1	0.2	0.4	0.8	1.6	3.2	6.4
	Grid spacing (mm)	0.392	0.784	1.569	3.137	6.275	12.549	25.098

of the initial aperture approximately coincides with a normal distribution with the same mean value and the same SD as those of the fracture for all fracture sizes. Although the PDF determined from the  $256 \times 256$  data is slightly scattered around that of the original data, they are essentially the same. Thus, the statistical properties were maintained after the grid spacing was enlarged, and this was also true for the sheared fractures. If synthetic fractures with the same PSDs of the surface height and aperture as those measured in the experiments are created with a small number of grid points, the statistical properties of the aperture are quite different from those described above since the aperture does not contain high-frequency components, as described in Section 3.3. Thus, it is necessary to create a synthetic fracture with small grid spacing even if the flow area is reconstructed with large grid spacing for simulating water flow.

However, a conical filter (4 points in the radial direction) had to be used to remove the components of the highest frequencies contained in sharp troughs since the solutions for the linear equations on pressure did not converge after several points were in contact due to the sharp troughs (see Matsuki et al. [7] for details). The SD of the initial aperture decreases with filtering, while the mean aperture maintains its original value. Therefore, to keep the SD of the initial aperture at the same value as with the original ( $256 \times 256$ ) data, the filtered aperture was enlarged around the mean value by multiplying by the ratio of the SDs of the non-filtered and filtered apertures. Thus, the components of the highest frequencies were ignored in the simulation of water flow. Therefore, we estimated the effect of filtering on the estimation of the permeability of all fractures that are normally closed to be in contact at a single point. The results showed that the permeability of the fractures slightly decreased with filtering, but the error was less than 2%. Accordingly, it can be said that filtering has only a small effect on the estimation of permeability. This is because the amplitude of the components with high frequencies is small relative to that of the components with low frequencies even for fractures without shear deformation (Fig. 9). The effect of filtering for sheared fractures is much smaller than that for normally closed fractures since the PSD of the non-filtered initial aperture at high frequencies is much smaller than that at low frequencies, as will be shown later in Figs. 30 and 31.

Thus, we simulated water flow by using aperture data with larger grid spacing but with the same statistical properties as those of the original fractures. This means that the percentage of the contact area produced in the flow area by a certain closure is essentially the same as that in the original fractures. Furthermore, we will estimate the hydraulic conductivity by using the hydraulic aperture, which is derived from the total volume flow rate (Eq. (27)) and therefore gives the mean hydraulic conductivity of the fracture even if the flow is heterogeneous. Thus, we believe that the trend of the mean hydraulic conductivity may be reasonably estimated even using a large grid spacing for the

flow area, although we obviously cannot obtain information on local flow in an area smaller than the grid spacing. Further discussion on the effects of grid spacing will be made later in comparison with the PSD of the initial aperture.

## 6. Results and discussion

### 6.2. Permeability of a fracture during normal closure

Fig. 17 shows the fracture size effect on the normalized hydraulic aperture  $e_h/e_m$  when the fracture is normally closed to have a mean aperture  $e_m$  of 0.65 and 0.7 mm. The results for fractures smaller than 0.2 m are also shown for comparison. The broken lines indicate the mean values of  $e_h/e_m$  determined for fracture sizes of from 0.2 to 12.8 m. Although the  $e_h/e_m$  values are scattered, the normalized hydraulic aperture is approximately independent of the fracture size when the fracture size is equal to or greater than 0.2 m, up until which point the normalized hydraulic aperture decreases with fracture size. Note that the normalized hydraulic aperture decreases with closure (with a decrease in  $e_m$ ). As described previously, the SD of the initial aperture increases with fracture size until the fracture size exceeds 0.2 m, but is almost constant beyond that point (Fig. 11). Accordingly, the size effect on the permeability of a fracture that is normally closed to have the same mean aperture almost disappears when the fracture is greater than 0.2 m, since the SD of the aperture is almost constant beyond this fracture size.

The decrease in the hydraulic aperture with fracture size is consistent with the experimental results obtained by Raven and Gale [8], as described previously. However, the large scatter in the normalized hydraulic aperture of large fractures with almost the same SD of the initial aperture

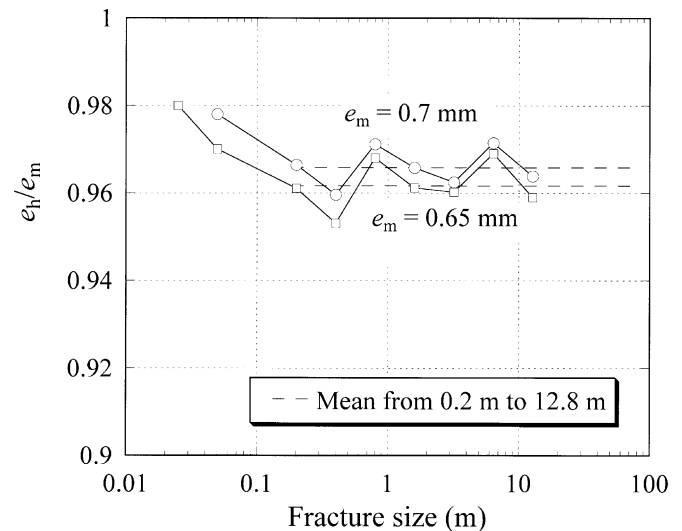


Fig. 17. Fracture size effect on the normalized hydraulic aperture  $e_h/e_m$  when the fracture is normally closed to have a mean aperture  $e_m$  of 0.65 and 0.7 mm.

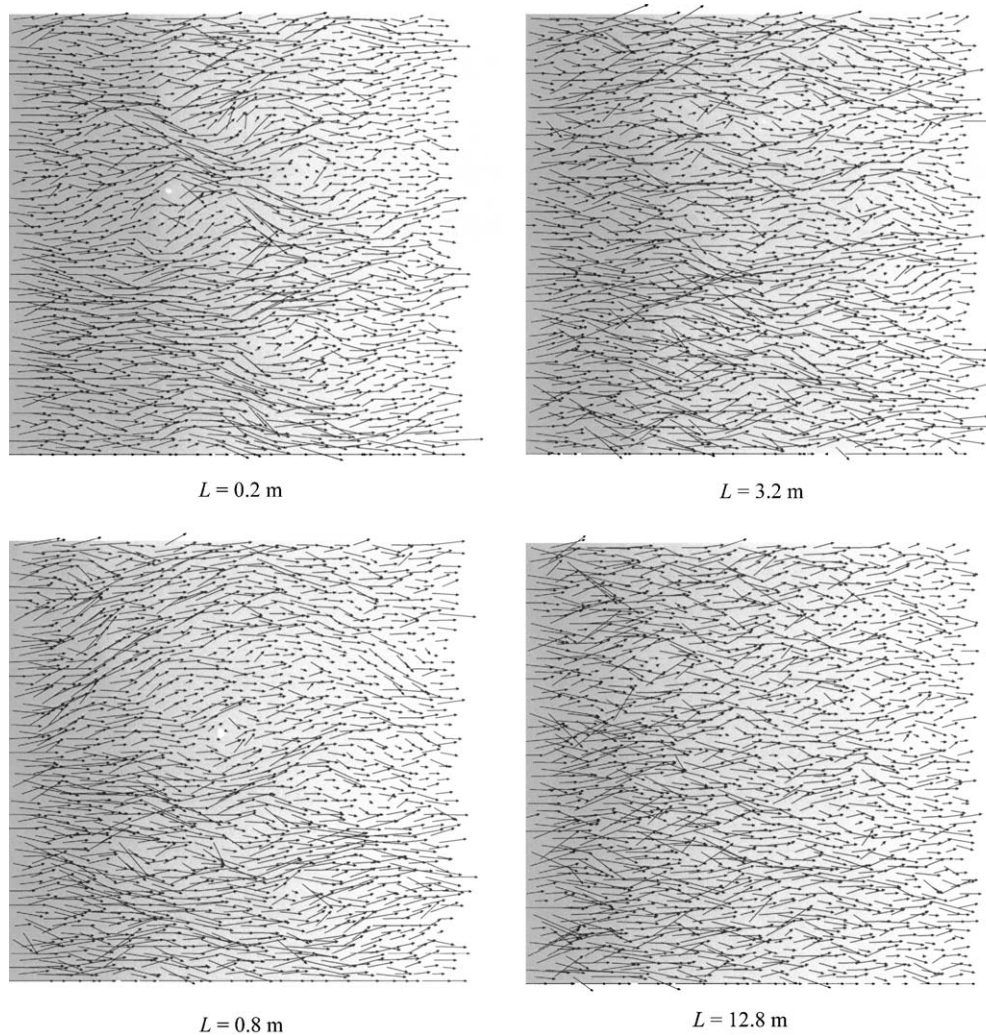


Fig. 18. Velocity and pressure fields for fracture sizes  $L$  of 0.2, 0.8, 3.2 and 12.8 m when they are closed to have a mean aperture  $e_m$  of 0.65 mm.

indicates that both the statistical properties of the aperture and also the layout of the aperture significantly affect the permeability of fractures. This suggests that it may be difficult to experimentally determine the size effect on the permeability of a fracture since an individual sample has a unique aperture layout. Thus, Gale [38] obtained experimental results inconsistent with those reported by Raven and Gale [8].

Fig. 18 shows the velocity and pressure fields for fracture sizes  $L$  of 0.2, 0.8, 3.2 and 12.8 m when they are closed to have a mean aperture  $e_m$  of 0.65 mm. The pressure is shown using a gray scale, where pressure decreases with brightness. The small white area indicates the area in contact, where the pressure cannot be defined. The data used for the velocity field represent only about 2.3% of those obtained at all grid points. Note that the same value for the macroscopic pressure gradient was used for all fractures so that a similar velocity could be obtained for fractures of various sizes. The flow is more or less tortuous for all fracture sizes, but no appreciable difference is observed among them. This is because the aperture distribution

relative to the fracture size is similar for all fracture sizes (Figs. 8 and 16).

Matsuki et al. [7] proposed Eq. (1) as a size-independent formula for estimating the normalized hydraulic aperture  $e_h/e_m$  of a hydraulic fracture with a size of less than 16 mm as a function of the mean aperture normalized by the SD of the initial aperture  $e_m/\sigma_0$ , as described previously. The relation between  $e_h/e_m$  and  $e_m/\sigma_0$ , obtained in this study, is summarized in Fig. 19 in comparison with Eq. (1). Although the relations obtained in this study for large fractures were scattered around the curve of Eq. (1), the mean relation can be given by Eq. (1). Accordingly, we can use Eq. (1) to estimate the permeability of a large fracture if the mean aperture and the SD of the initial aperture are determined. Thus, the normalized hydraulic aperture of a fracture during normal closure is determined by the mean aperture relative to the SD of the initial aperture, and appreciably decreases with closure. When the mean aperture is 8, 4, 2 and 1 times the SD of the initial aperture, the hydraulic aperture is 99.1%, 96.6%, 88.8% and 70.2% of the mean aperture, respectively, which corresponds to

97.1%, 90.2%, 70.1% and 34.6% of the volume flow rate, respectively. Thus, the hydraulic aperture is greater than 99% of the mean aperture when the mean aperture is greater than 7.7 times the SD of the initial aperture.

6.2. Permeability of a fracture during closure after shearing

Fig. 20 shows the effect of the fracture size on the normalized hydraulic aperture  $e_h/e_m$  when the fracture is sheared by  $\delta = 12.5, 25$  and  $50$  mm and is closed to have a mean aperture  $e_m$  of  $4.0$  mm. Solid symbols indicate the normalized hydraulic aperture for macroscopic flow

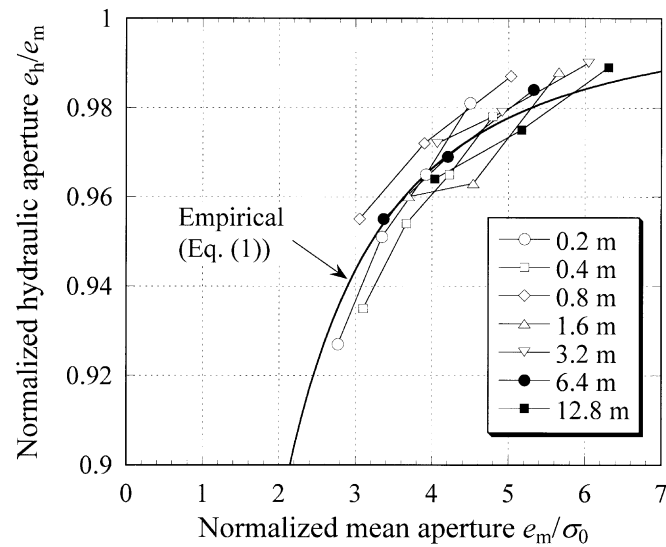


Fig. 19. Relation between  $e_h/e_m$  and  $e_h/\sigma_0$  obtained for synthetic fractures without shearing in comparison with Eq. (1).

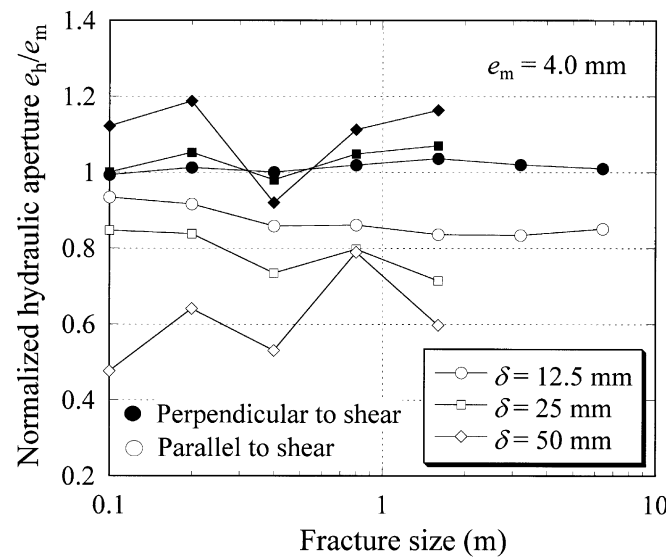


Fig. 20. Effect of fracture size on the normalized hydraulic aperture  $e_h/e_m$  when the fracture is sheared by  $\delta = 12.5, 25$  and  $50$  mm and is closed to have a mean aperture  $e_m$  of  $4.0$  mm.

perpendicular to the shear displacement and open symbols indicate that parallel to the shear displacement. For  $\delta = 25$  and  $50$  mm, pressure could not be calculated for the largest fractures of  $3.2$  and  $6.4$  m when the fractures were closed to have a mean aperture of  $4.0$  mm. First, the permeability of a fracture subjected to shear displacement shows remarkable anisotropy, as previously reported in laboratory experiments on small fractures [10,12]. The normalized hydraulic aperture  $e_h/e_m$  in the macroscopic flow parallel to the shear displacement is less than 1, and is much smaller than that in the macroscopic flow perpendicular to the shear displacement, which is mostly greater than 1. Furthermore, this anisotropy in the permeability increases with an increase in shear displacement when the fractures are closed to have the same mean aperture. In particular, the normalized hydraulic aperture in the macroscopic flow parallel to the shear displacement significantly decreases with shear displacement. Since we could not obtain the hydraulic aperture for large fractures and also since the results showed a large scatter due to the effects of the layout of the aperture for each fracture, the fracture size effects cannot be clearly seen in Fig. 20.

The relations between  $e_h/e_m$  and  $e_m/\sigma_0$  obtained by all flow analyses are shown in Fig. 21 for each shear displacement. The average relation given by Eq. (1) for the normalized hydraulic aperture of the fracture during normal closure is also shown for comparison. The value of  $e_h/e_m$  in the macroscopic flow parallel to the shear displacement (with a decrease in  $e_m/\sigma_0$ ) while that in the macroscopic flow perpendicular to the shear displacement (solid symbols) mostly increases with closure. Thus, the anisotropy in the hydraulic conductivity of the sheared fracture increases with closure. The  $e_h/e_m$  versus  $e_m/\sigma_0$  plot obtained for the fracture during normal closure is located between those for the two directions of macroscopic flow in sheared fractures. Thus, for a given normalized mean aperture, the normalized hydraulic aperture in the macroscopic flow perpendicular to the shear displacement is greater than that of a fracture without shearing while that in the macroscopic flow parallel to the shear displacement is mostly smaller than that of a fracture without shearing.

Fig. 22 shows these diagrams for fracture sizes  $L$  of  $0.1, 0.2, 0.8$  and  $1.6$  m. The anisotropy in the hydraulic conductivity of a sheared fracture increases as the shear displacement increases for small fractures ( $L = 0.1$  and  $0.2$  m). However, the effect of shear displacement on the relation between  $e_h/e_m$  and  $e_m/\sigma_0$  decreases with fracture size and almost disappears when the fracture size equals  $1.6$  m, at which point the magnitude of a shear displacement of  $50$  mm relative to the fracture size is about  $3.1\%$ . Fig. 23 shows the relation between  $e_h/e_m$  and  $e_m/\sigma_0$  for (a)  $\delta > 0.031 L$  and (b)  $\delta < 0.031 L$ . When  $\delta > 0.031 L$  (9 of 21 cases), the relations are scattered due to the dependence on the shear displacement relative to the fracture size ( $\delta/L = 0.06-0.5$ ). However, when  $\delta < 0.031 L$  (12 cases), the scatter is greatly reduced and similar relations are obtained

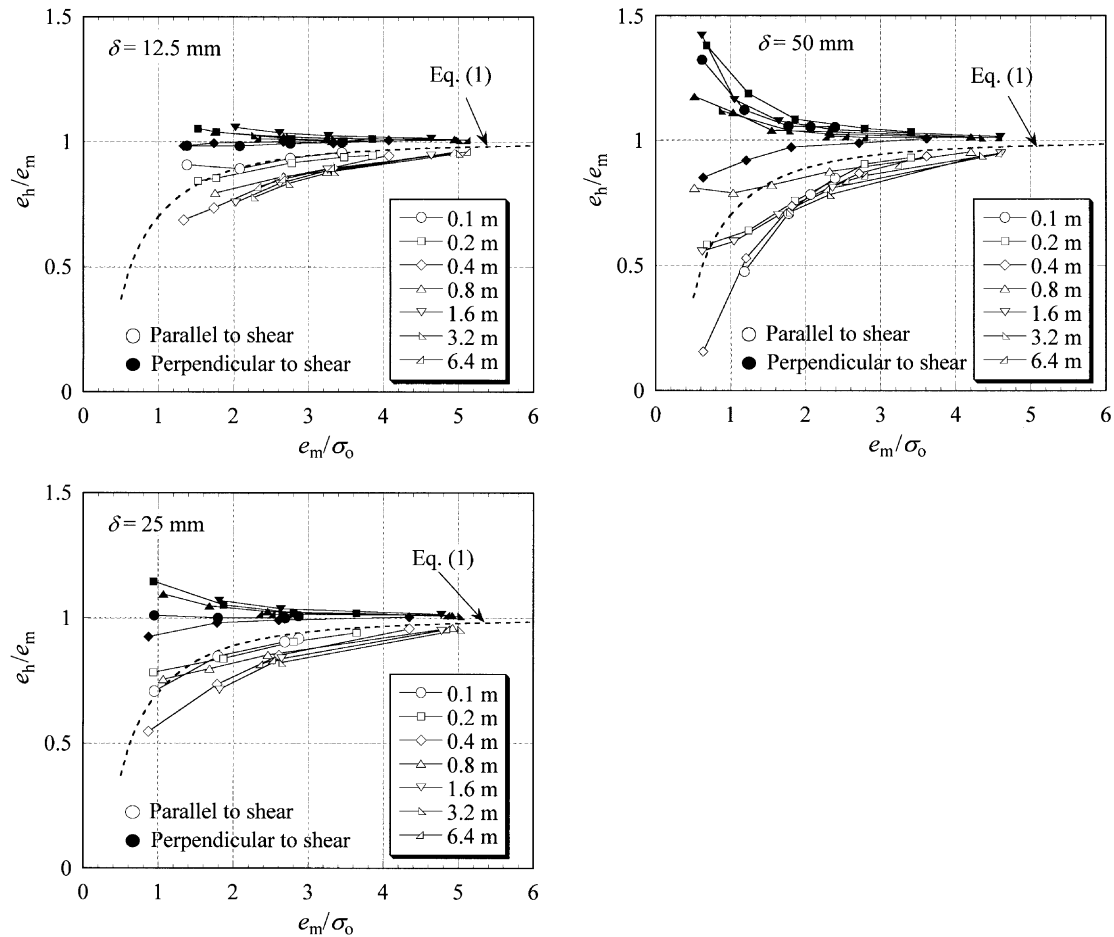


Fig. 21. Relation between  $e_h/e_m$  and  $e_m/\sigma_0$  for each shear displacement.

regardless of both the fracture size and the shear displacement. Thus, for a given fracture size, the relation between the normalized hydraulic aperture and the normalized mean aperture is approximately independent of the shear displacement until the shear displacement exceeds about 3.1% of the fracture size. For a given shear displacement, the relation depends on the fracture size until the fracture size exceeds about 32 times the shear displacement, beyond which the SD of the initial aperture is almost independent of the fracture size (Fig. 13). Thus, the fracture size effect on the relation between the normalized hydraulic aperture and the normalized mean aperture almost disappears when the SD of the initial aperture is independent of the fracture size. This indicates that the SD of the initial aperture also governs water flow in sheared fractures.

Fig. 24 shows the velocity and pressure fields for the two directions of macroscopic flow and the aperture distribution when fractures of 0.1, 0.2, 0.4 and 1.6 m in size are sheared by 12.5 mm and closed to have a mean aperture of 4.0 mm. The scale beneath the middle figures indicates the magnitude of the shear displacement for reference. The contour maps of the aperture distribution are given at every 1 mm, and brighter parts indicate areas with a greater

aperture. Although the number of grid points in the velocity field was greatly reduced (about 4.9% of all points) for clarity, the contour maps of the aperture were determined using the values at all grid points ( $256 \times 256$ ). Those for a shear displacement of 25 and 50 mm are shown in Figs. 25 and 26, respectively. Clearly, channeling flow develops in the macroscopic flow perpendicular to the shear displacement, although it is also observed in the macroscopic flow parallel to the shear displacement. However, in the latter case, the flow is inhibited more as the shear displacement increases. The flow is more localized as the shear displacement increases or as the fracture size decreases. Furthermore, the number of channels tends to increase with the fracture size and decrease with the shear displacement for fractures that are equal to or smaller than 1.6 m. Thus, for these fractures, the flow pattern is governed by the magnitude of the shear displacement relative to the fracture size. Flow channeling is important for the practical problems related to contaminant transport in geologic systems [39].

Fig. 27 shows the velocity and pressure fields in the direction of the macroscopic flow perpendicular to the shear displacement when large fractures of 3.2 and 6.4 m are sheared by 12.5 mm and closed to have a mean aperture

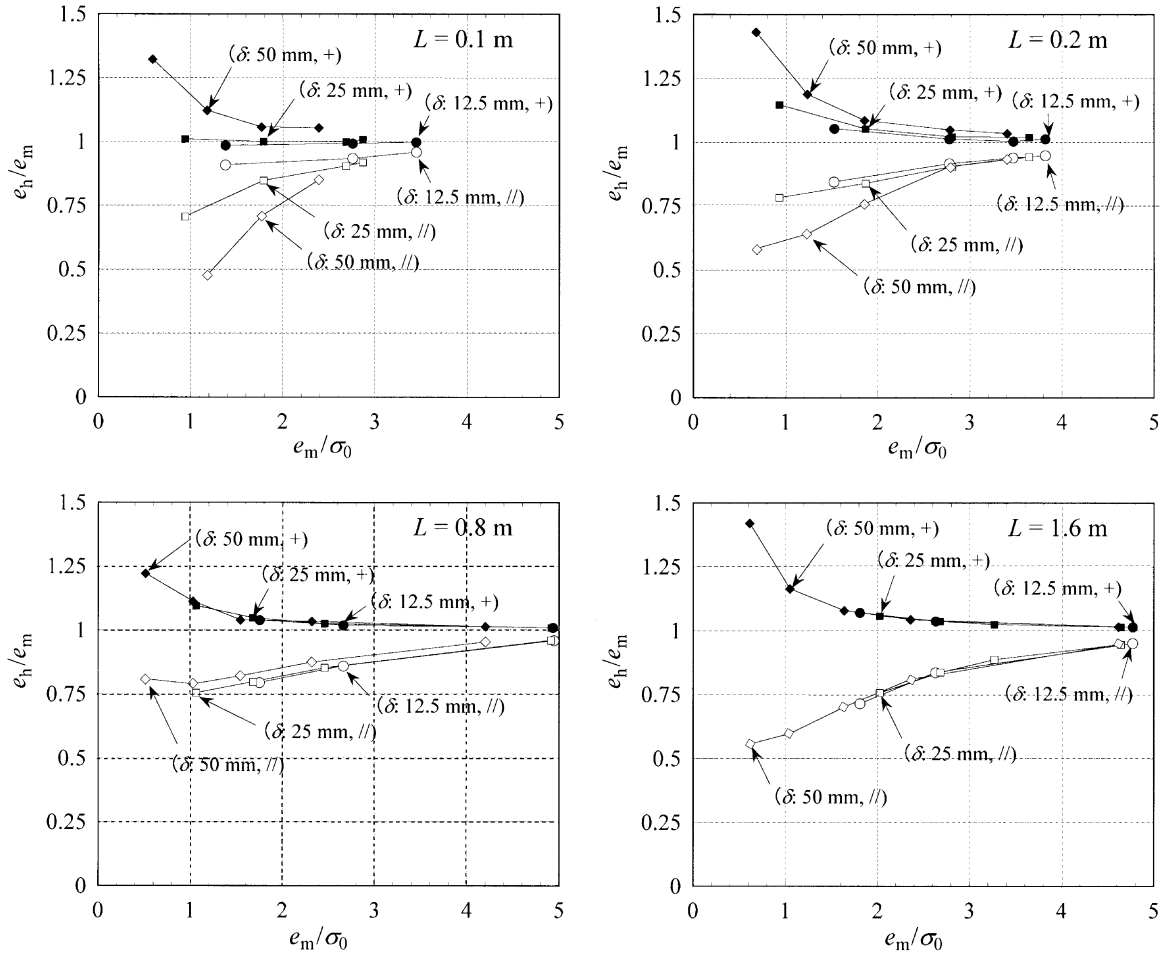


Fig. 22. Relation between  $e_h/e_m$  and  $e_m/\sigma_0$  for fracture sizes  $L$  of 0.1, 0.2, 0.8 and 1.6 m.

$e_m$  of 4.0 mm. One-sixteenth of the flow area is enlarged and is shown beneath each figure. For the whole flow area, the number of grid points in the velocity field was increased to about 9.2% of all grid points, which is almost the upper limit for being able to clearly see the velocity field, while the velocity vectors at all grid points are shown for the one-sixteenth part of the flow area to see local flow more precisely. Although channeling flow develops, the tendency described above for small fractures is not clearly observed in these large fractures. Thus, the number of predominant channeling flows no longer appears to increase with fracture size.

It is obvious that large apertures are connected to each other to form a channel, which results in the development of channeling flow. As described previously, shear displacement reduces the degree of matedness between the two fracture surfaces and, as a result, the magnitudes of the components of an aperture with low frequencies (large wavelengths) increase relative to those with high frequencies, particularly for small fractures (Fig. 12). Thus, the probability of the connectivity of large apertures greatly increases with shear displacement and, accordingly, channels may be easily created in sheared fractures. In contrast, the connectivity is poor for the aperture of a fracture

without shearing, since, as can be seen in Fig. 8, large apertures exist almost at random and are interrupted by small apertures between them.

The number of grid points that are in contact significantly increases with shear displacement when fractures are closed to have the same mean aperture, since the SD of the initial aperture significantly increases with shear displacement (Fig. 13). The percentage of points in contact is 0.2–0.7%, 3–6% and 11–18% of all grid points for  $\delta = 12.5, 25$  and  $50$  mm, respectively, when the fractures are closed to have a mean aperture of 4.0 mm. Fig. 28 shows areas where the aperture is smaller than 1.0 mm in black for all shear displacements, when fractures of 0.1, 0.4, 1.6 and 6.4 m are closed to have a mean aperture of 4.0 mm. We call an area that forms an isolated island a ridge. The ridges contain points in contact and water flows through channels that may form between ridges. Fig. 28 clearly shows that ridges and channels form approximately perpendicular to the shear displacement. Thus, the ridges inhibit the macroscopic flow parallel to the shear displacement [13] and at the same time channeling flow develops in the macroscopic flow perpendicular to the shear displacement. Since these effects of the channels and ridges in the aperture become more remarkable with closure of the fracture,

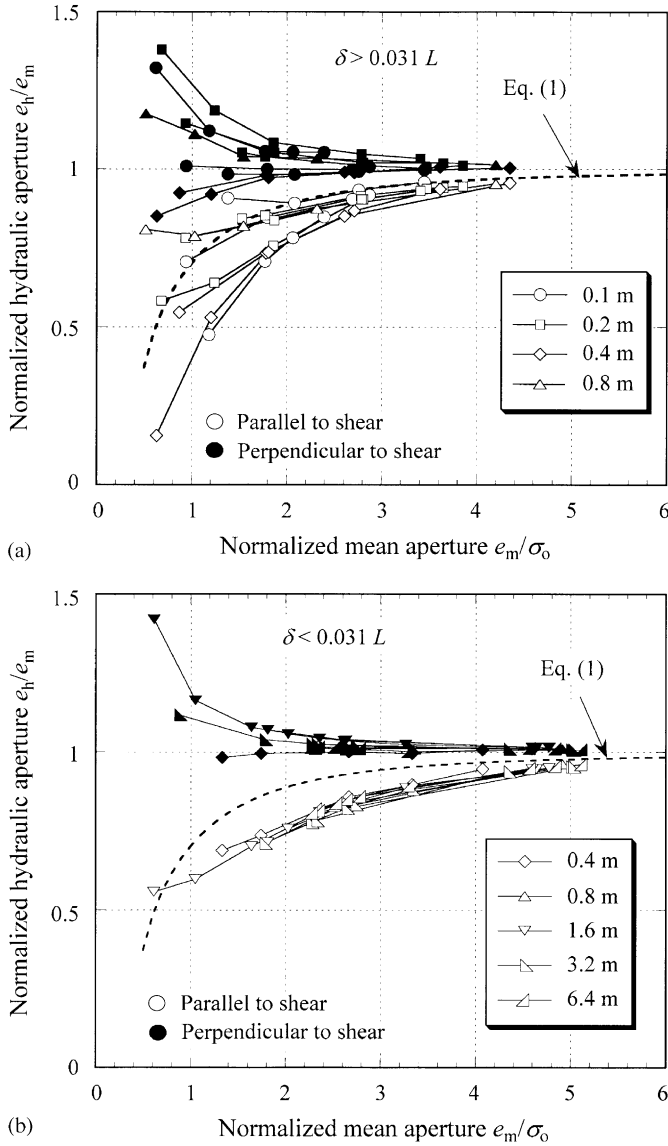


Fig. 23. Relation between  $e_h/e_m$  and  $e_m/\sigma_0$  for (a)  $\delta > 0.031 L$  and (b)  $\delta < 0.031 L$ .

the anisotropy in the permeability of the sheared fracture increases with closure. When a large fracture of, for example, 6.4 m is sheared by 25 and 50 mm, only narrow channels relative to the fracture size are produced, which makes it difficult to determine the hydraulic aperture.

Fig. 28 also shows that the number of ridges increases with the fracture size. Accordingly, ridges and channels form in a more dispersed manner relative to the fracture size as the fracture size increases. This suggests that the number of channeling flows may increase with the fracture size even in a flow area of  $256 \times 256$  grid points and that the effects of the heterogeneous flow may be averaged to give the mean conductivity of large fractures. On the other hand, while the number of ridges increases when shear displacement increases from 12.5 to 25 mm, it decreases when shear displacement increases from 25 to 50 mm, since a greater number of small ridges are connected to each other to form

a large ridge. Thus, the flow is greatly localized for  $\delta = 50$  mm, since a large percentage of contact points are connected to each other to form large ridges. The localization of water flow in a sheared fracture suggests that the permeability of a sheared fracture should not be estimated by that in a narrow area, since the permeability at one point can be quite different from that at another point. In fact, Hanano [40] reported an experience in a geothermal field where a well that intersected a fracture showed sufficient steam production while another well that intersected the same fracture at a distance of less than 10 m from the first well produced almost no steam.

Fig. 29 shows the distribution of apertures greater than the mean aperture (channels) in white when fractures of 0.1, 0.2, 0.8 and 1.6 m were sheared by 50 mm and closed to have a mean aperture of 4.0 mm. The normalized hydraulic apertures of these fractures in the macroscopic flow perpendicular to the shear displacement are greater than 1.1. Clearly, a few predominant channels with a depth greater than the mean aperture are created perpendicular to the shear displacement for these fractures. The volume flow rate is proportional to the cubed aperture when the flow is assumed to be that in a parallel-plates model (Eq. (27)) [1]. This means that a single channel with a small width but a large aperture can provide a conduit for water flow through which a greater volume of water flows than that provided by the parallel-plates model with the mean aperture.

### 6.3. Aperture PSD of a sheared fracture

Let us first consider the effect of shear displacement on the Fourier components of the aperture when the shear displacement  $\delta (>0)$  is given in the  $X$ -direction. For convenience, we consider a completely mated fracture with identical surfaces. The height of the upper surface  $h_1(x, y)$  given by Eq. (4) can be rewritten by the following discrete inverse Fourier transform:

$$h_1(x, y) = \sum_{k=0}^{N-1} \sum_{l=0}^{N-1} a_{kl} e^{i2\pi(k(x/L)+l(y/L))}, \quad (28)$$

where  $a_{kl}$  is a complex Fourier component for the spatial frequencies  $k/L$  and  $l/L$  in the  $X$ - and  $Y$ -directions, respectively,  $L \times L$  is the fracture size and  $N \times N$  is the number of grid points. The height of the lower surface  $h_2(x, y)$  is obtained by shifting Eq. (28) by  $\delta$  in the  $X$ -direction since the lower surface was assumed to originally be the same as the upper surface.

$$h_2(x, y) = \sum_{k=0}^{N-1} \sum_{l=0}^{N-1} a_{kl} e^{i2\pi(k((x-\delta)/L)+l(y/L))}. \quad (29)$$

Accordingly, the aperture  $e(x, y)$  created by these surfaces is obtained by taking the difference between Eqs. (28) and (29).

$$e(x, y) = \sum_{k=0}^{N-1} \sum_{l=0}^{N-1} e_{kl} e^{i2\pi(k(x/L)+l(y/L))}, \quad (30)$$

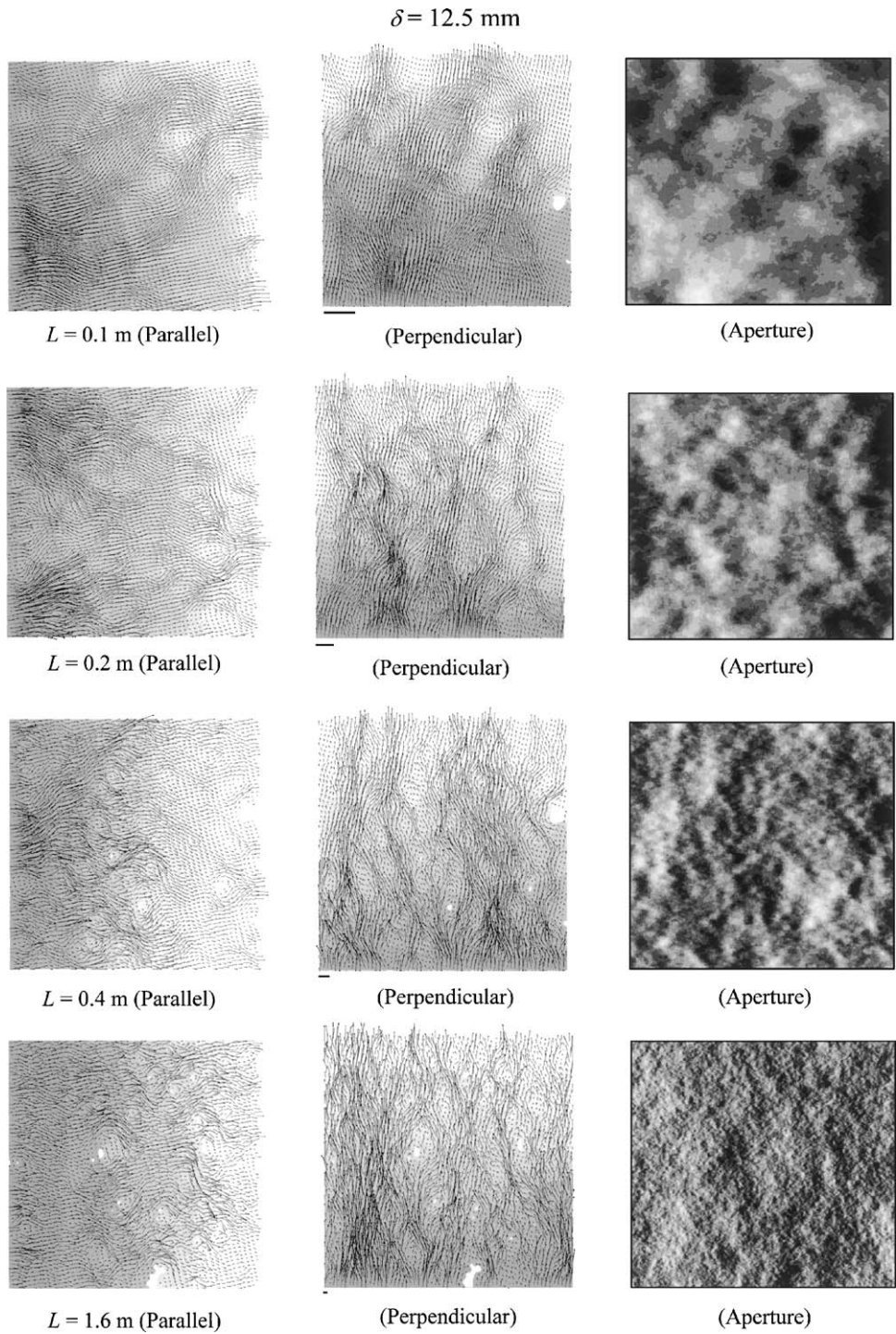


Fig. 24. Velocity and pressure fields for two directions of macroscopic flow and the aperture distribution when fractures of 0.1, 0.2, 0.8 and 1.6 m in size are sheared by 12.5 mm and is closed to have the mean aperture of 4.0 mm.

where the Fourier component of the aperture  $e_{kl}$  is given by

$$e_{kl} = 2 \sin\left(\pi k \frac{\delta}{L}\right) a_{kl} e^{i\pi(1/2 - k(\delta/L))}. \quad (31)$$

The initial aperture is obtained by adjusting a constant component of Eq. (30) so that the two surfaces may be in contact at a single point.

The linear profiles of the height of the upper surface in the  $X$ - and  $Y$ -directions,  $h(x)$  and  $h(y)$ , respectively, are obtained from Eq. (28) for a given value of  $y$  and  $x$ , respectively.

$$h(x) = \sum_{k=0}^{N-1} c_k^h e^{i2\pi k(x/L)}, \quad h(y) = \sum_{l=0}^{N-1} c_l^h e^{i2\pi l(y/L)}, \quad (32)$$

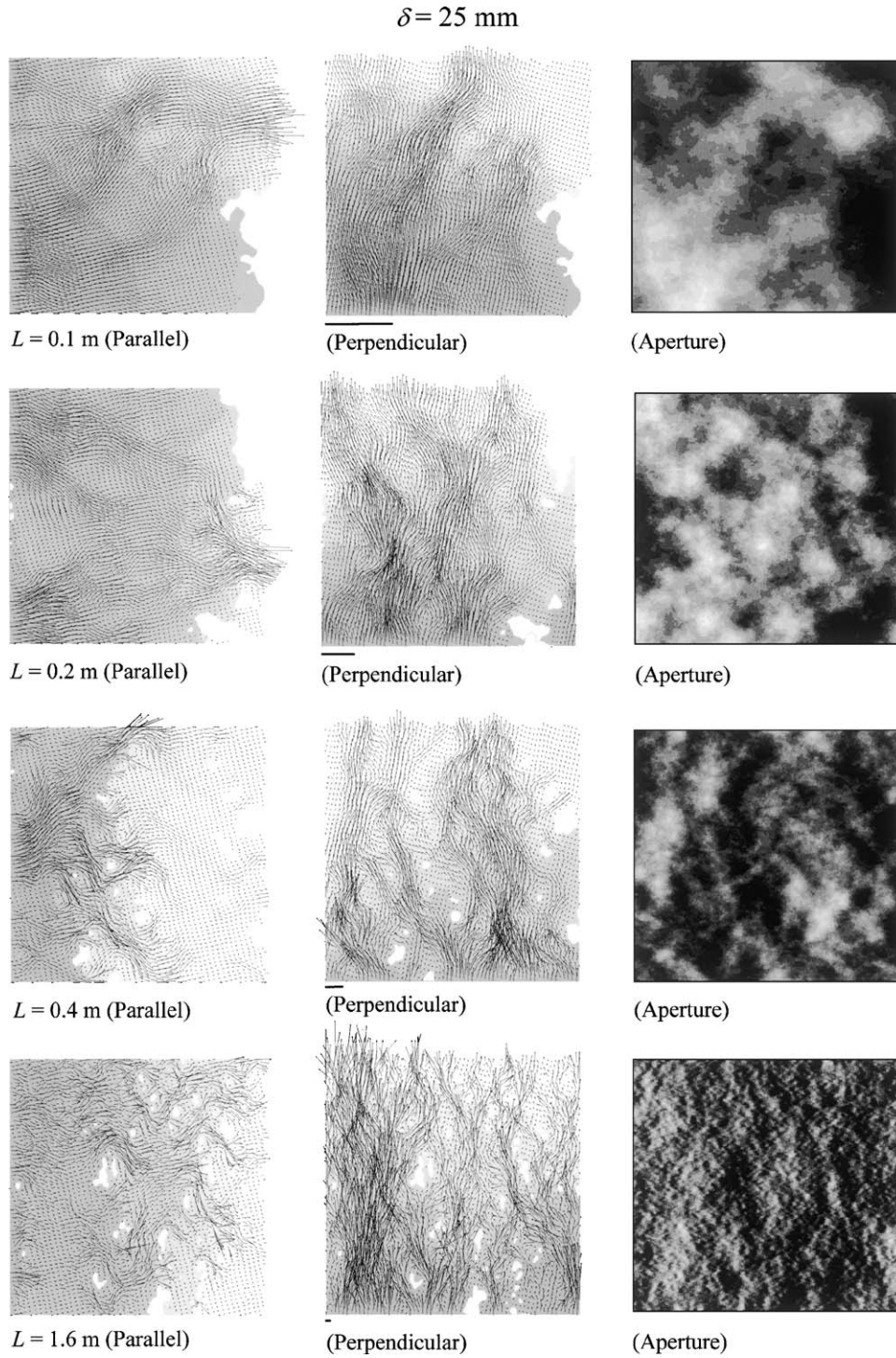


Fig. 25. Velocity and pressure fields for two directions of macroscopic flow and the aperture distribution when fractures of 0.1, 0.2, 0.8 and 1.6 m are sheared by 25 mm and closed to have a mean aperture of 4.0 mm.

where

$$c_k^h = \sum_{l=0}^{N-1} a_{kl} e^{i2\pi l(y/L)}, \quad c_l^h = \sum_{k=0}^{N-1} a_{kl} e^{i2\pi k(x/L)}. \quad (33)$$

Similarly, the linear profiles of the aperture in the X- and Y-directions,  $e(x)$  and  $e(y)$ , respectively, is

obtained from Eq. (30) for a given value of  $y$  and  $x$ , respectively.

$$e(x) = \sum_{k=0}^{N-1} c_k^e e^{i2\pi k(x/L)}, \quad e(y) = \sum_{l=0}^{N-1} c_l^e e^{i2\pi l(y/L)}, \quad (34)$$

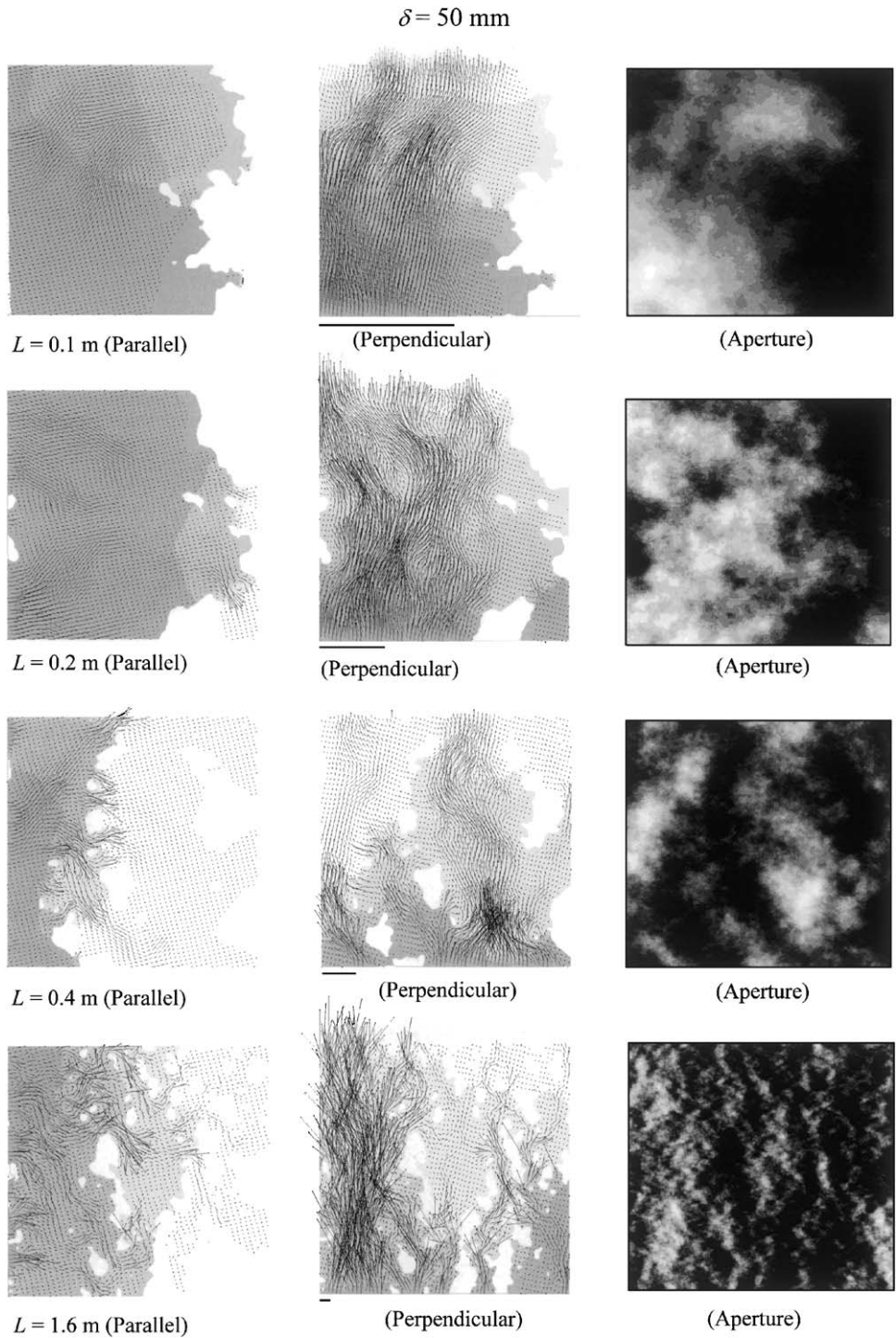


Fig. 26. Velocity and pressure fields for two directions of macroscopic flow and the aperture distribution when fractures of 0.1, 0.2, 0.8 and 1.6 m are sheared by 50 mm and closed to have a mean aperture of 4.0 mm.

where

$$c_k^e = 2 \sin\left(\pi k \frac{\delta}{L}\right) e^{i\pi(1/2-k(\delta/L))} \sum_{l=0}^{N-1} a_{kl} e^{i2\pi l(y/L)},$$

$$c_l^e = 2 \sum_{k=0}^{N-1} \sin\left(\pi k \frac{\delta}{L}\right) e^{i\pi(1/2-k(\delta/L))} a_{kl} e^{i2\pi k(x/L)}.$$

(35)

From Eqs. (33) and (35), for the direction parallel to the shear displacement (the  $X$ -direction), the Fourier component of the aperture  $c_k^e$  can be related to that of the height of the upper surface  $c_k^h$  for an arbitrary value of  $y$  as

$$c_k^e = 2 \sin\left(\pi k \frac{\delta}{L}\right) e^{i\pi(1/2-k(\delta/L))} c_k^h. \tag{36}$$

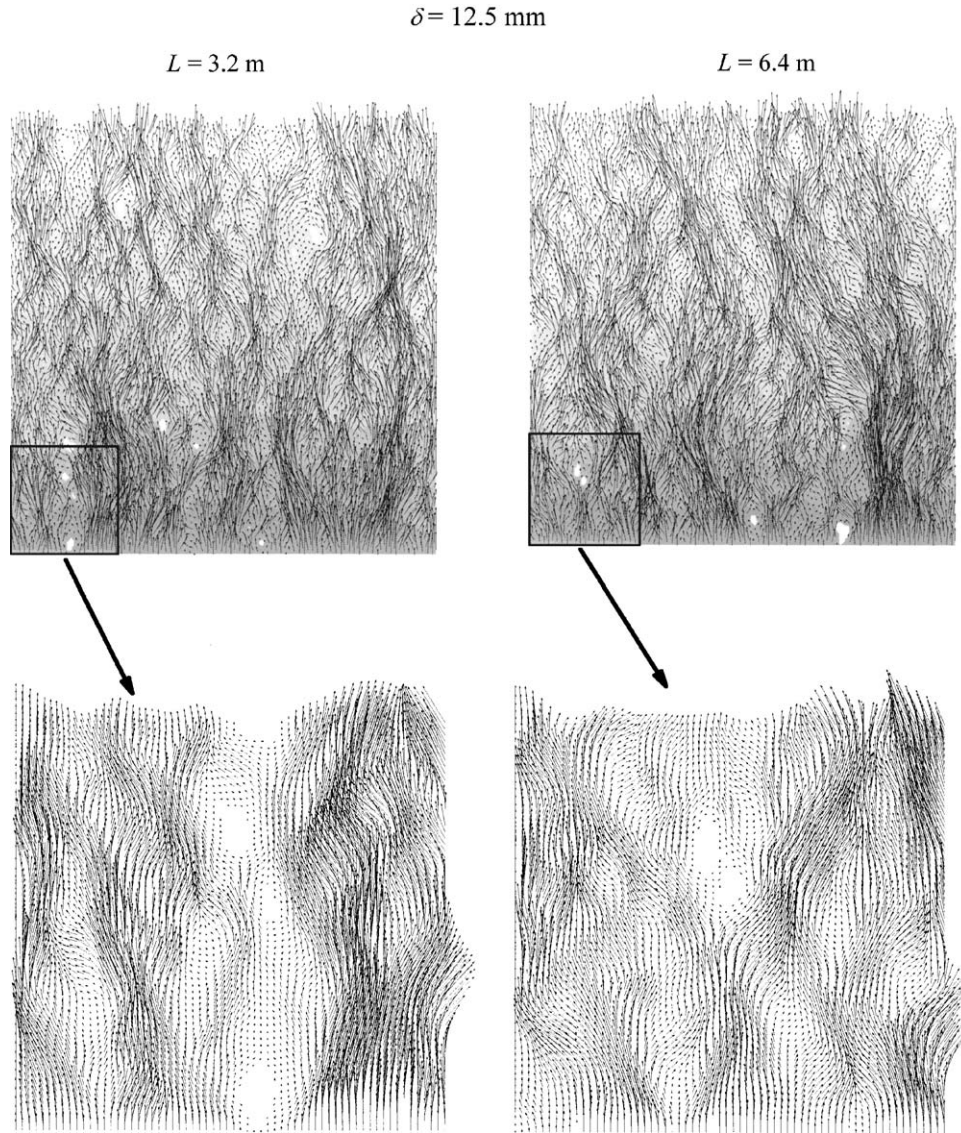


Fig. 27. Velocity and pressure fields for macroscopic flow perpendicular to the shear displacement when fractures of 3.2 and 6.4 m are sheared by 12.5 mm and closed to have a mean aperture of 4.0 mm.

Thus, the amplitude of the aperture in the direction parallel to the shear displacement is given for the spatial frequency  $k/L$  by

$$|c_k^e| = 2|c_k^h| \left| \sin\left(\frac{\pi k \delta}{L}\right) \right| \quad (k = 1, N - 1). \quad (37)$$

Accordingly, the PSD of the aperture in the direction parallel to the shear displacement  $G_{ex}(f)$  is given by

$$G_{ex}(f) = 2G(f)\{1 - \cos(2\pi\delta f)\}, \quad (38)$$

where  $G(f)$  is the PSD of the surface height and  $f = k/L$ . The above equation coincides with that obtained by Wang et al. [41] using the autocorrelation function. Eq. (37) means that the amplitude of the Fourier component of the aperture in the shear direction varies periodically relative to that of the surface height according to the shear displacement  $\delta$  unless  $\delta$  is zero, for which no apertures are

produced. Thus, the PSD of the aperture relative to that of the surface height of a sheared fracture is locally maximum and has a value of 4 when

$$\frac{k}{L} = \frac{1}{\delta} \left( n + \frac{1}{2} \right) \quad (n = 0, 1, \dots), \quad (39)$$

and is locally minimum and has a value of zero when

$$\frac{k}{L} = \frac{1}{\delta} n \quad (n = 0, 1, \dots). \quad (40)$$

However, a real fracture has surfaces more or less different from each other and therefore the Fourier component of the aperture is never zero. Thus, oscillation of the amplitude of the Fourier components of the aperture occurs with a spatial frequency of  $1/\delta$ , with the first local maximum at  $1/(2\delta)$ , when the aperture of a linear profile is considered. Note that we did not

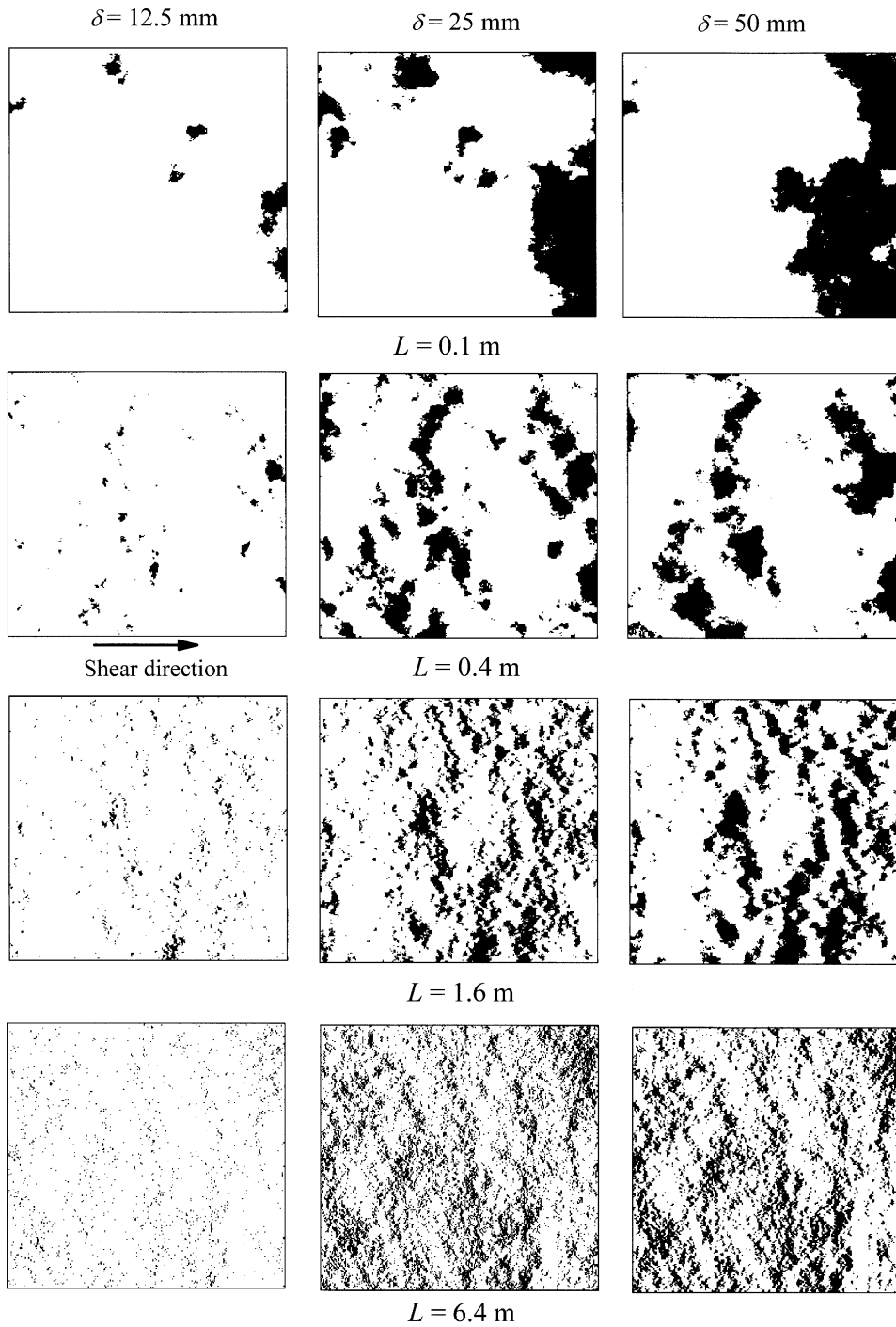


Fig. 28. Effects of both fracture size and shear displacement on the formation of ridges in the aperture when fractures of 0.1, 0.4, 1.6 and 6.4 m are sheared by  $\delta$  and closed to have a mean aperture of 4.0 mm.

consider the difference in the relative phases among linear profiles.

For the direction perpendicular to the shear displacement (the  $Y$ -direction), the Fourier component of the aperture is not directly related to those of the surface height for an arbitrary value of  $x$ . Therefore, to know the relation between the PSDs of the surface height and the aperture in

the  $Y$ -direction, it is necessary to take an average of the PSD for all values of  $x$  by

$$\overline{G(f)} = \frac{1}{L} \int_0^L |c_i^h|^2 dx, \quad \overline{G_{ey}(f)} = \frac{1}{L} \int_0^L |c_i^e|^2 dx, \quad (41)$$

where the former is the average PSD of the height of the upper surface, the latter is that of the aperture and  $f = l/L$ .

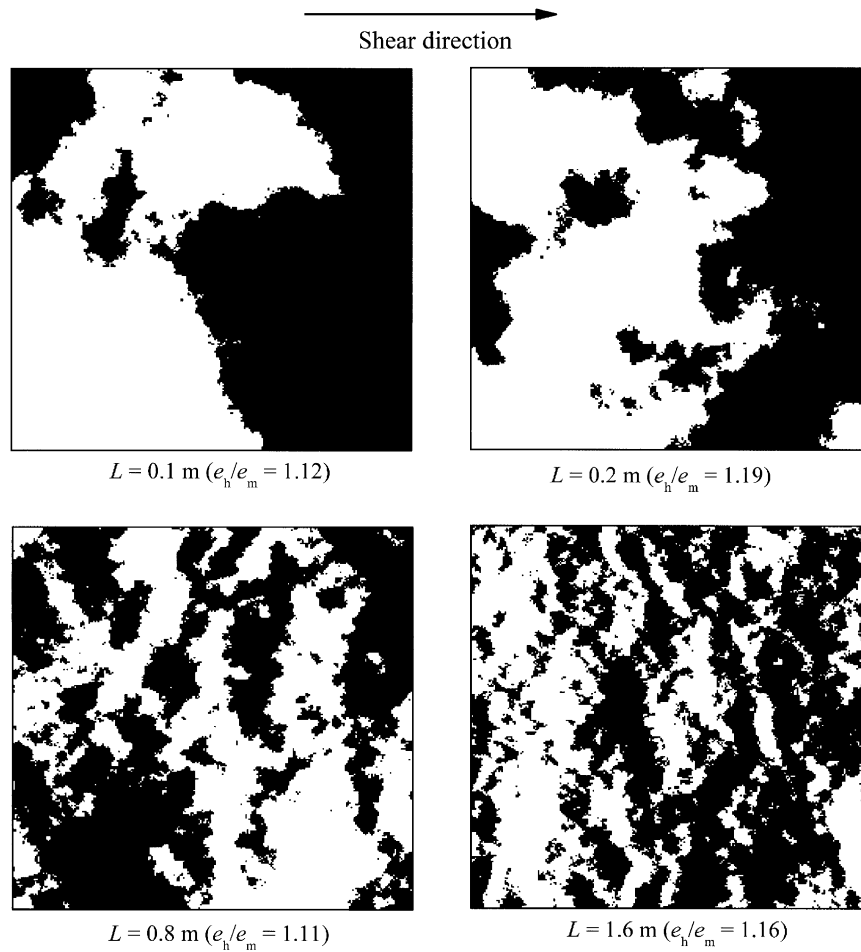


Fig. 29. Distribution of apertures greater than the mean aperture (channel) when fractures of 0.1, 0.2, 0.8 and 1.6 m are sheared by 50 mm and closed to have a mean aperture of 4.0 mm.

As a result, the following equations were obtained by using the amplitude of the Fourier component  $a_{kl}$  of the height of the upper surface:

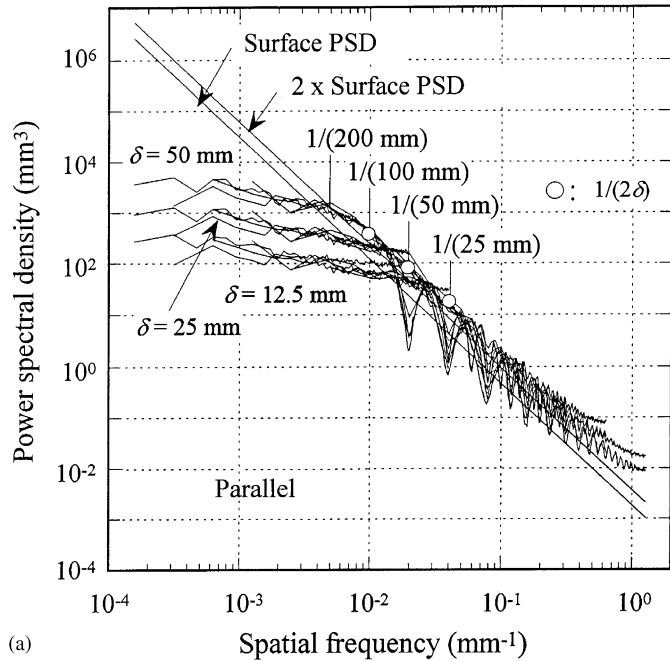
$$\overline{G(f)} = \sum_{k=0}^{N-1} |a_{kl}|^2, \quad \overline{G_{ey}(f)} = \sum_{k=0}^{N-1} 4 \sin^2\left(\pi k \frac{\delta}{L}\right) |a_{kl}|^2. \quad (42)$$

The former is given by Eq. (2) (power law) and the latter is an asymptote at twice the former although we do not know an explicit form for the latter.

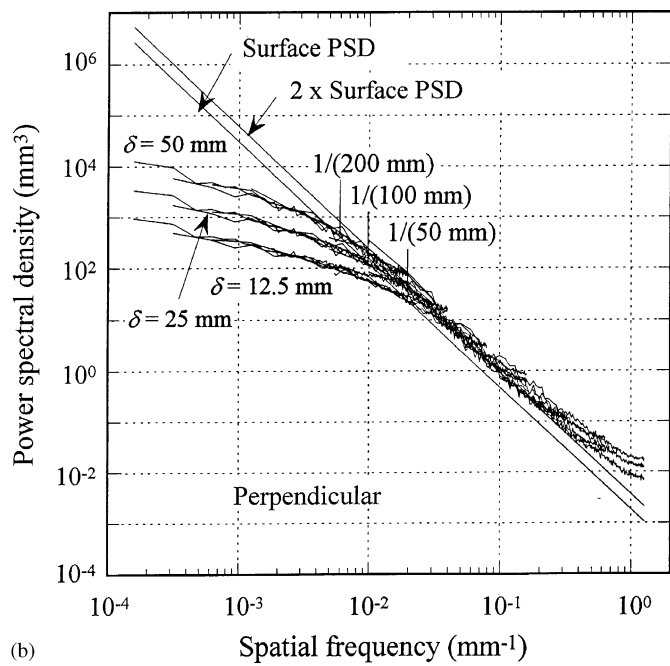
Fig. 30 shows the ensemble-averaged PSDs of the linear profiles of the initial aperture for all synthetic fractures when the fracture is sheared by 12.5, 25 and 50 mm. Fig. 30(a) shows the PSD in the shear direction and Fig. 30(b) shows that perpendicular to the shear direction. The PSD of the surface height together with that multiplied by two are also shown for comparison. The PSD of the initial aperture was determined for the non-filtered data of  $256 \times 256$  grid points to clearly show the effect of shear displacement. Note that the deviation of the initial aperture PSD from a line of twice the surface height PSD at high frequencies is due to an error in FFT. For all shear displacements, the PSD of the initial aperture in the shear

direction is twice that of the surface height at a spatial frequency of  $1/(4\delta)$  and has a first local maximum relative to the PSD of the surface height at a spatial frequency of  $1/(2\delta)$ , as indicated by open circles, beyond which the PSD of the initial aperture rapidly decreases with the spatial frequency, with the same slope as that of the PSD of the surface height, but oscillating with a frequency of  $1/\delta$ , as theoretically considered above. In contrast, the PSD in the direction perpendicular to the shear direction coincides with that of the surface height at a spatial frequency of about  $1/(4\delta)$  and shows an asymptote at twice the PSD of the surface height with an increase in spatial frequency, as theoretically considered above.

The effect of shear displacement on the PSD of the initial aperture both parallel and perpendicular to the shear displacement is summarized in Fig. 31. The PSD of the initial aperture in the direction parallel to the shear displacement (solid line) is determined by Eq. (38) since it approximately gives the actual one, excluding local minima, and that in the direction perpendicular to the shear displacement (broken line) is determined by calculating Eq. (42). The solid circles indicate the PSDs at a wavelength of  $10\delta$  and the open circles for the direction



(a)



(b)

Fig. 30. Ensemble-averaged PSD of linear profiles of the initial aperture in the directions (a) parallel and (b) perpendicular to the shear displacement for all fracture sizes when the fracture is sheared by 12.5, 25 and 50 mm.

parallel to the shear displacement indicate those at a wavelength of  $2\delta$ . The PSDs of the initial apertures of all fractures without shearing, the maximum wavelength in the flow area ( $256 \times 256$  points) of sheared fractures and the maximum grid spacing in the simulation of water flow (25.098 mm for a fracture of 6.4 m) are also shown for reference. The PSDs of the aperture when sheared fractures are closed to have a mean aperture of 4.0 mm are smaller than those of the initial aperture, but this difference is not

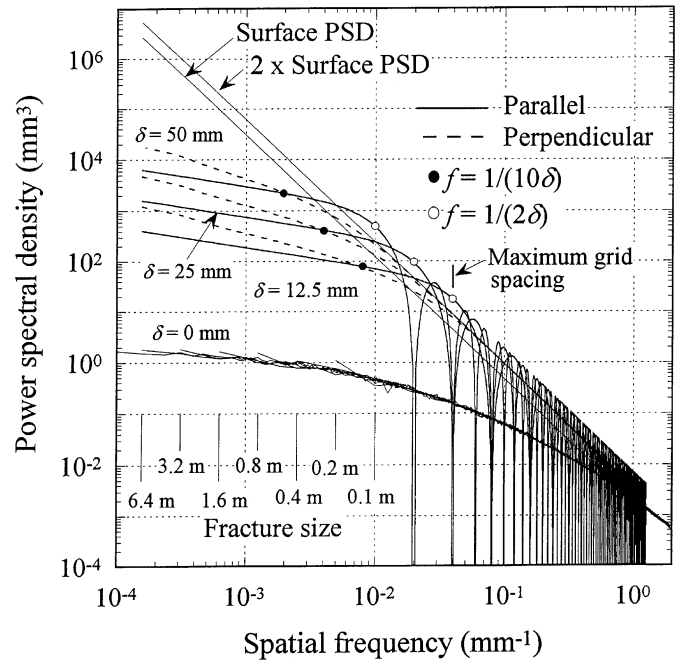


Fig. 31. Effect of shear displacement on the PSD of the initial aperture.

significant. Therefore, we can discuss the aperture of sheared fractures with a mean aperture of 4.0 mm using this figure.

The PSD of the initial aperture significantly increases with shear displacement for both directions. Accordingly, the magnitude of the aperture in the channels increases and that in the ridges decreases with shear displacement. As a result, the hydraulic aperture of a sheared fracture in the macroscopic flow perpendicular to the shear displacement increases with shear displacement while that in the macroscopic flow parallel to the shear displacement decreases with shear displacement when the fractures are closed to have the same mean aperture (Fig. 20).

The important feature in the PSD of the initial aperture of a sheared fracture is that the PSD of the aperture has a much greater value for wavelengths greater than  $2\delta$  than for wavelengths less than  $2\delta$  for both directions. This means that a large aperture is produced only with wavelengths greater than  $2\delta$ . Thus, large channels in the aperture may be produced only with wavelengths greater than  $2\delta$  for any fracture size. The value of  $2\delta$  when  $\delta = 12.5$  mm is almost identical to the maximum grid spacing used in the simulation of water flow, 25.098 mm for a sheared fracture of 6.4 m, below which the PSD of the aperture rapidly decreases with spatial frequency. Accordingly, it can be said that the grid spacing used in this study had only a small effect on the estimation of the conductivity of the sheared fractures since the amplitudes of the components with wavelengths of smaller than 25 mm are small. Furthermore, for all shear displacements, the PSD of the initial aperture in the direction parallel to the shear displacement is greater than that perpendicular to

the shear displacement for wavelengths greater than  $2\delta$  and less than about  $10\delta$  ( $2\delta < \lambda < 10\delta$ ) and is smaller than that for wavelengths greater than about  $10\delta$  ( $\lambda > 10\delta$ ). Thus, the initial aperture distribution of the sheared fracture is never isotropic. Obviously, if the PSD of the aperture is the same for an arbitrary direction, the aperture distribution is isotropic like that of normally closed fractures, for which channeling flow does not occur preferably in any direction. In contrast, when a difference in the PSD of the aperture exists between the two directions, this produces anisotropy in the aperture distribution and may produce channels and ridges perpendicular to the direction with greater PSD. Accordingly, channels and ridges with  $2\delta < \lambda < 10\delta$  may be created perpendicular to the shear displacement while those with  $\lambda > 10\delta$  may also be created parallel to the shear direction, depending on the maximum wavelength that equals the size of the fracture. Actually, the number of channeling flows in the macroscopic flow parallel to the shear displacement is smaller than that perpendicular to the shear displacement (Figs. 24 and 25), although channeling flow is not clearly observed for the macroscopic flow parallel to the shear displacement since flow is inhibited by the ridges.

However, the above discussion only applies to the amplitude spectrum of the linear profiles of the aperture and therefore the effect of the phase difference among the linear profiles was not taken into consideration. The Fourier component of the aperture contains a relative phase that is distributed at random for any wavelength. Accordingly, even if we pay attention only to a component with a certain wavelength, the position of the local maximum in the aperture in each linear profile differs by a distance less than the wavelength. Therefore, the channels of the aperture form depending on the phase differences among linear profiles for each wavelength. Thus, the channels created by the shear displacement are more or less tortuous and sometimes connected to each other or branch off, as shown in Figs. 24–27.

If the fracture size ( $L$ ) is not much greater than  $2\delta$ , as is the case for small fractures less than 0.4 m, the wavelengths of the aperture for the creation of channels are limited to a narrow region. Accordingly, for small fractures a small number of channels may form perpendicular to the shear direction and the number of channels may increase with the fracture size and decrease with shear displacement (Figs. 24–26 and Fig. 28). In contrast, when the fracture size is much greater than  $2\delta$ , as in the case of large fractures greater than 1.6 m, all of the components with wavelengths of  $2\delta < \lambda < 10\delta$  are superposed to form channels regardless of the fracture size. Thus, the tendency for the number of channels to increase with the fracture size was not clearly observed for large fractures. Furthermore, for small fractures, a large portion of the PSD of the initial aperture is occupied by wavelengths less than  $2\delta$  and this portion increases with shear displacement. Accordingly, the aperture distribution of small fractures more closely resembles the surface of a fracture with an increase in shear

displacement (Fig. 12). In contrast, as the fracture size increases, a portion of the PSD of the initial aperture is occupied more by wavelengths greater than  $2\delta$ . Accordingly, the aperture distribution of large fractures resembles that of normally closed fractures (Fig. 12).

Figs. 30 and 31 show that the PSD of the initial aperture increases only slightly with an increase in wavelength for wavelengths greater than  $2\delta$  for all shear displacements. Therefore, similar to the discussion given by Brown [26] for the fracture size effect on the SD of the aperture of a normally closed fracture, the SD of the initial aperture of a sheared fracture increases with fracture size to quickly asymptote a certain value, depending on the shear displacement. Thus, the fracture size effect on the SD (of linear profiles) of the initial aperture of sheared fractures disappears at a certain fracture size that increases with shear displacement, as already described in association with Fig. 13.

## 7. Conclusions

To estimate the size effect on the aperture and permeability of a large fracture, synthetic fractures of from 0.2 to 12.8 m were created on a computer by a new spectral method. The fracture size effect on the standard deviation of the initial aperture was first analyzed for fractures both with and without shearing. Next, by taking aperture data at intervals to establish a flow area, water flow was simulated for fractures during both normal closure and closure after shearing, by solving Reynolds equation to determine the hydraulic aperture normalized by the mean aperture as a measure of the permeability of the fracture. The main conclusions in this study can be summarized as follows:

- (1) The spectral method proposed in this study for creating a synthetic fracture approximately reproduced the ratio of the PSD of the initial aperture to that of the surface height, determined for a tensile fracture of 1 m.
- (2) When the fracture is closed without shearing to have the same mean aperture, the fracture size effect on the hydraulic aperture disappears when the fracture size exceeds about 0.2 m, since beyond this size the standard deviation of the initial aperture is almost independent of the fracture size. An empirical formula was proposed to estimate the hydraulic aperture of a fracture of any size by giving the mean aperture and the standard deviation of the initial aperture.
- (3) When the fracture is closed after shearing, the hydraulic conductivity shows remarkable anisotropy. The hydraulic aperture in the macroscopic flow perpendicular to the shear displacement is much greater than that in the macroscopic flow parallel to the shear displacement. The former is mostly greater than the mean aperture and the hydraulic aperture normalized by the mean aperture increases with closure, while the latter is mostly less than the mean aperture and the normalized

hydraulic aperture decreases with closure. This anisotropy increases with the shear displacement when the fracture is closed to have the same mean aperture.

- (4) The relation between the hydraulic aperture normalized by the mean aperture and the mean aperture normalized by the standard deviation of the initial aperture is approximately independent of both the fracture size and shear displacement when the shear displacement is less than about 3.1% of the fracture size, where the standard deviation of the initial aperture of the sheared fracture is almost independent of the fracture size.
- (5) The channels and ridges that form perpendicular to the shear displacement cause the anisotropy in the hydraulic conductivity of a sheared fracture. The PSD of the aperture of a sheared fracture significantly increases with shear displacement. As a result, the magnitudes of channels in the aperture increase with shear displacement and accordingly the anisotropy in the permeability of a sheared fracture with the same mean aperture becomes more remarkable as shear displacement increases. Furthermore, the power spectral density of the aperture of a sheared fracture has a much greater value for wavelengths greater than two times the shear displacement than that for wavelengths less than twice the shear displacement, and that in the shear direction is greater than that in the direction perpendicular to the shear displacement for wavelengths of from 2- to 10-fold the shear displacement. Accordingly, channeling flow develops perpendicular to the shear direction and the number of channels increases with fracture size and decreases with shear displacement for small fractures.

## References

- [1] U.S. National Committee for Rock Mechanics. Rock fractures and fluid flow. National Academy Press; 1996. 551p.
- [2] Lomize GM. Water flow through jointed rock. Moscow: Gosenergoizdat; 1951 127p.
- [3] Brown SR. Fluid flow through rock joints: the effect of surface roughness. *J Geophys Res* 1987;92:1337–47.
- [4] Brown SR. Transport of fluid and electric current through a single fracture. *J Geophys Res* 1989;94:9429–38.
- [5] Thompson ME, Brown SR. The effect of anisotropic surface roughness on flow and transport in fractures. *J Geophys Res* 1991;96:21923–32.
- [6] Amadei B, Illangsekare T. A mathematical model for flow and transport in non-homogeneous rock fractures. *Int J Rock Mech Min Sci Geomech Abstr* 1994;31:719–31.
- [7] Matsuki K, Lee JJ, Sakaguchi K. Size effect in flow conductance of a closed small-scale hydraulic fracture in a granite. *Geotherm Sci Technol* 1999;6:113–38.
- [8] Raven KG, Gale JE. Water flow in a natural rock fracture as a function of stress and sample size. *Int J Rock Mech Min Sci Geomech Abstr* 1985;22:251–61.
- [9] Olsson WA, Brown SR. Hydraulic response of a fracture undergoing compression and shear. *Int J Rock Mech Min Sci Geomech Abstr* 1993;30:845–51.
- [10] Esaki T, Du S, Mitani Y, Ikusada K, Jing L. Development of a shear-flow test apparatus and determination of coupled properties for a single rock joint. *Int J Rock Mech Min Sci* 1999;36:641–50.
- [11] Yeo IW, De Freitas MH, Zimmerman RW. Effect of shear displacement on the aperture and permeability of a rock fracture. *Int J Rock Mech Min Sci* 1998;35:1051–70.
- [12] Matsuki K, Sakaguchi K, Inoue Y. Analysis of shear dilation and permeability of a hydraulic fracture in granite. *Proceedings of the 9th international congress on rock mechanics, Paris; 1999. p. 765–8.*
- [13] Mitani Y, Esaki T, Nakashima Y. An experimental study on the anisotropy of flow in a rock joint. *Proceedings of the 2002 ISRM regional symposium on rock engineering, Seoul, Korea; 2002. p. 281–8.*
- [14] Fardin N. The effect of scale on the morphology, mechanics and transmissivity of single rock fractures. Dr. thesis, Stockholm, Sweden; 2003.
- [15] Kranz RL, Frankel AD, Engelder T, Scholz CH. The permeability of whole and jointed Barre granite. *Int J Rock Mech Min Sci Geomech Abstr* 1979;16:225–34.
- [16] Witherspoon PA, Wang JSY, Iwai K, Gale JE. Validity of cubic law for fluid flow in a deformable rock fracture. *Water Resour Res* 1980;16:1016–24.
- [17] Tsang YW, Witherspoon PA. Hydromechanical behavior of a deformable rock fracture subject to normal stress. *J Geophys Res* 1981;86:9287–98.
- [18] Kojima T, Nomura T, Matsuki K. A fundamental study on permeability of granites under simulated geothermal conditions. *J Geothermal Res Soc Jpn* 1994;16:25–39 [in Japanese with English abstract].
- [19] Kojima T, Murai T, Matsuki K. An experimental study on normal stiffness and flow conductance of a small-scale hydraulic fracture in a granite. *J Geothermal Res Soc Jpn* 1995;17:285–95 [in Japanese with English abstract].
- [20] Wang EQ, Sakaguchi K, Okumura K, Matsuki K. Time-dependent closure and permeability of a small-scale hydraulic fracture under constant normal stress. *Proceedings of the World Geothermal Congress (CD-ROM); 2000. p. 3951–56.*
- [21] Brown SR, Scholz CH. Broad bandwidth study of the topography of natural rock surfaces. *Geophys Res Lett* 1985;90:12575–82.
- [22] Power WL, Tullis TE, Brown SR, Boitnott GN, Scholz CH. Roughness of natural fault surfaces. *Geophys Res Lett* 1987;14:29–32.
- [23] Brown SR. A note on the description of surface roughness using fractal dimension. *Geophys Res Lett* 1987;14:1095–8.
- [24] Power WL, Tullis TE, Weeks JD. Roughness and wear during brittle faulting. *J Geophys Res* 1988;93:15268–78.
- [25] Power WL, Durham WB. Topography of natural and artificial fractures in granitic rocks: implications for studies of rock friction and fluid migration. *Int J Rock Mech Min Sci Geomech Abstr* 1997;34:979–89.
- [26] Brown SR. Simple mathematical model of rough fracture. *J Geophys Res* 1995;100:5941–52.
- [27] Sakaguchi K, Tomono J, Okumura K, Ogawa Y, Matsuki K. Size effect on surface height and aperture distributions of a fracture. *J Geotherm Res Soc Jpn* 2002;24:149–60 [in Japanese with English abstract].
- [28] Saupe D. Algorithms for random fractals. In: Peitgen H-O, Saupe D, editors. *The science of fractal images*. New York: Springer; 1988. p. 71–136.
- [29] Brown SR, Kranz RL, Bonner BP. Correlation between the surfaces of natural rock joints. *Geophys Res Lett* 1986;13:1430–3.
- [30] Matsuki K, Kojima T, Murai T. Surface roughness and initial aperture distribution of a small-scale fracture in granite. *J Geotherm Res Soc Jpn* 1995;17:213–32 [in Japanese with English abstract].
- [31] Glover PWJ, Matsuki K, Hikima R, Hayashi K. Synthetic rough fractures in rocks. *J Geophys Res* 1998;103:9609–20.
- [32] Glover PWJ, Matsuki K, Hikima R, Hayashi K. Fluid flow in fractally rough synthetic fractures. *Geophys Res Lett* 1997;14:1803–6.

- [33] Glover PWJ, Matsuki K, Hikima R, Hayashi K. Fluid flow in synthetic rough fractures and application to the Hachimantai geothermal HDR test site. *J Geophys Res* 1998;103:9621–35.
- [34] Mandelbrot BB. *The fractal geometry of nature*. New York: Freeman; 1983 486p.
- [35] Peitgen H-O, Saupe D, editors. *The science of fractal images*. New York: Springer; 1988 445p.
- [36] Brown SR, Stockman HW, Reeves SJ. Applicability of Reynolds equation for modeling fluid flow between rough surfaces. *Geophys Res Lett* 1995;22:2537–40.
- [37] Pyrak-Nolte LJ, Cook NGW, Nolte DD. Fluid percolation through single fractures. *Geophys Res Lett* 1988;15:1247–50.
- [38] Gale J. Hydraulic behaviour of rock joints. *Proceedings of the international symposium on rock joints*, Leon, Norway; 1990. p. 351–62.
- [39] Tsang CF, Neretnieks I. Flow channeling in heterogeneous fractured rocks. *Rev Geophys* 1988;36:275–98.
- [40] Hanano M. Two roles of fractures in geothermal development: contribution to occurrence of geothermal resources and well production. *J Geotherm Res Soc Jpn* 2000;22:107–16 [in Japanese with English abstract].
- [41] Wang JSY, Narasimhar TN, Scholz CH. Aperture correlation of a fractal fracture. *J Geophys Res* 1988;93:2216–24.